

# FINAL PUBLISHABLE JRP REPORT

JRP-Contract number	ENG61	
JRP short name	FutureGrid	
JRP full title	Non-conventional voltage and current sensors for future power grids	
Version numbers of latest contracted Annex Ia and Annex Ib against which the assessment will be made	Annex Ia:	V1.1
	Annex Ib:	V1.01
Period covered (dates)	From 1 June 2014	To 31 May 2017
JRP-Coordinator		
Name, title, organisation	Jari Hällström, Dr., VTT (MIKES until 31.12.2014)	
Tel:	+358 50 382 2127	
Email:	jari.hallstrom@vtt.fi	
JRP website address	<a href="http://futuregrid.emrp.eu/">http://futuregrid.emrp.eu/</a>	
Other JRP-Partners		
Short name, country	CMI, Czech Republic FFII, Spain LNE, France METAS, Switzerland PTB, Germany SMU, Slovakia RISE, Sweden TUBITAK, Turkey VSL, Netherlands	
REG1-Researcher (associated Home Organisation)	John Nelson STRATH, United Kingdom	Start date: 1 <sup>st</sup> June 2014 Duration: 36 months
REG2-Researcher (associated Home Organisation)	Peter Schegner TUD, Germany	Start date: 1 <sup>st</sup> January 2015 Duration: 29 months
REG3-Researcher (associated Home Organisation)	Pontus Johannisson Chalmers, Sweden	Start date: 1 <sup>st</sup> November 2014 Duration: 12 months

**Report Status: PU Public**

**TABLE OF CONTENTS**

1	Executive Summary.....	3
2	Project context, rationale and objectives.....	4
	2.1 Context.....	4
	2.2 Objectives.....	4
3	Research results.....	5
	3.1 Current sensor based on Faraday effect in optical fibre .....	5
	3.1.1 The Faraday effect .....	5
	3.1.2 Fibre development .....	6
	3.1.3 Testing of the interferometric system .....	6
	3.1.4 Theory and modelling of the phase modulation system .....	7
	3.1.5 Phase modulation designs: open-air and all- fibre systems .....	8
	3.1.6 Conclusion .....	9
	3.2 Magnetic shielding technique for a Rogowski coil .....	9
	3.3 Precision voltage sensor for medium voltage networks.....	13
	3.4 New non-conventional sensor techniques .....	15
	3.4.1 Current clamp.....	15
	3.4.2 Interrogation using fibre Bragg grating.....	16
	3.5 Testing of the developed sensors .....	19
	3.5.1 Laboratory testing of the developed Rogowski coil .....	19
	3.5.2 Medium voltage testing of voltage probe .....	20
	3.5.3 Medium voltage testing of the current clamp .....	21
	3.5.4 Laboratory testing of the fibre Bragg grating based sensors.....	22
	3.6 New calibration services for sensors with analogue output .....	23
	3.6.1 Modified conventional test-set .....	24
	3.6.2 Sampler system .....	24
	3.6.3 Test-set for non-conventional sensors.....	25
	3.7 New calibration services for sensors with digital output .....	26
	3.7.1 Calibration of sensors with digital output .....	26
	3.7.2 Test-sets for calibration of sensors with digital output.....	27
	3.8 Conclusion.....	29
4	Actual and potential impact .....	31
	4.1 Dissemination.....	31
	4.2 Metrological achievements.....	31
	4.3 Early impact.....	31
	4.3.1 User uptake .....	31
	4.3.2 Standards .....	32
	4.4 Potential impact.....	32
5	Website address and contact details.....	33
	5.1 Project website address: <a href="http://futuregrid.emrp.eu/">http://futuregrid.emrp.eu/</a> .....	33
	5.2 Contact details.....	33
6	List of publications .....	34

## 1 Executive Summary

### Introduction

The drive for renewable and low carbon energy in Europe has led to more distributed energy sources, such as wind farms and solar power, being connected to the power network. The increased number of distributed sources means two-way flow of electricity (e.g. from the customer side back into the grid) which can affect power quality and cause power quality degradation or blackouts. Hence, accurate and traceable measurements are a necessity to control the additional demands of future power grids. Many existing measurement instruments are approaching the end of their life span, and they are not designed for a distributed network where power may flow from customer side. This project looked at non-conventional technologies that have the potential to be developed into new instruments capable of collecting more detailed information on the state of the power grid, to both replace current measurement transformers and monitor and control future power grids.

### The Problem

Europe is increasingly adopting alternative energy sources that have lower emissions and therefore contribute to meeting the EU's Horizon 2020 target of a 20 % of reduction in greenhouse gas emissions. The European power network is also evolving fast and the nature of measurements required is changing. The connection of these distributed renewable energy sources to the electrical transmission grid means two-way flow of electricity and may lead to more harmonics (where the sinusoidal wave of the alternating current (AC) is altered) in the transmitted waveform, which can impact power quality.

The first generation of measurement systems installed in the European power network are becoming obsolete. Traditional instrument transformers often only work well for measurement of the fundamental (50 Hz or 60 Hz) frequency, and their performance is not good enough for measurement of power harmonics generated by distributed power sources. Therefore, there are new requirements for the measurement infrastructure for the power network in order to enable reliable and robust control and billing in future power networks.

Several novel, non-conventional voltage and current sensor technologies have shown great promise in enabling transportable, accurate measurement for power network harmonics. They are different types of sensors, which have the potential to replace traditional measurement transformers of medium and high voltage power lines. National Metrology Institutes (NMI) also need to be able to provide accurate calibration of new wider bandwidth sensors required for power quality measurements on medium and high voltage networks. However, at the start of the project, these technologies lacked the level of accuracy needed and were not mature enough for wider application for on-site calibration or power quality measurements on high voltage grids.

### The Solution

This project set out to support wider application of novel sensor technologies in future power networks. This required the development, improvement and assessment of a number of new methods and instruments capable of collecting more diversified information on the state of the power grid than currently used transformers. The studied technologies indicated potential to replace traditional ones for control and billing in future power grids.

### Impact

The main impact from the project is the provision of new services, which have been established for calibration of digital and non-conventional voltage and current transformers. The calibration services will provide a means for manufacturers to prove the performance of their new products. Services were developed for both analogue and digital non-conventional current and voltage sensors, and respective test sets.

Wider application was found for the new technologies developed during the project: I) The project triggered development of new type of sensing fibre for optical current transformers. II) Work towards commercialisation of a medium voltage probe developed in the project is ongoing; and plans exist for using it as reference measurement device in follow-up project. III) The developed Rogowski coil was used for on-site calibration of customer's medium voltage current transformer. IV) A number of non-conventional sensors have already been calibrated for customers, based on the services introduced by this project. V) Feedback was provided to a commercial device manufacturer, in order to fix issues in the device software. VI) Development of a commercial version of openable Rogowski coil for measurements on medium voltage network was supported. VII) Development of shielding for Rogowski coil using ferromagnetic materials near the coil was supported.

## 2 Project context, rationale and objectives

### 2.1 Context

The drive for increased reliance on renewable or low carbon energy in Europe has led to more distributed energy sources such as wind farms and solar power systems being connected to the power network, leading to an increase in harmonics on the waveforms. The need to determine these harmonic voltages and currents poses new requirements for the measurement infrastructure associated with the generation, delivery, and protection of the electrical network. Both the bandwidth of these traditional instrument transformers and the capabilities of the current measurement and communication network do not match that of modern low voltage instrumentation.

Furthermore, the first generation of measurement systems installed in the European power network is getting old and the systems are being replaced. There is therefore a need to ensure that appropriate technology is available that enables reliable and robust control and billing in future power networks.

New, non-conventional technologies based for example on optical Faraday or Pockels effects, Rogowski coils, or upgrading of conventional instrument transformers with digital or optical readouts are being more and more widely applied. These solutions are potential replacements for traditional instrument transformers for power frequency measurement on medium and high voltage power lines, and they show great promise in enabling lightweight, accurate measurement systems for voltage and current, both for fundamental and harmonic frequencies. However, before this project the traceability for the measurement of harmonics was missing. This project set up to study the possibilities of novel non-conventional sensors, e.g. optical Faraday effect based sensors, hybrid electrical/optical sensors and air core Rogowski coils for current measurement; and voltage divider based systems for voltage measurement. Many of these technologies are already applied and promise wider bandwidth and lighter weight, but they are not yet of the required metrological accuracy. This project aimed to extend the accuracy of these technologies and to facilitate their wider acceptance.

### 2.2 Objectives

The overall aim of the project was to support wider application of novel sensor technologies in future power networks. The first four objectives looked at different technologies, which were then calibrated and tested on real networks in the final two objectives:

1. Design, manufacture and characterise a wideband sensor based on the optical Faraday Effect for traceable calibration of non-conventional and conventional current sensors on medium and high voltage networks. The target uncertainty for current measurement is below 100  $\mu\text{A}/\text{A}$ .
2. Apply a magnetic shielding technique to a Rogowski coil to improve its applicability for onsite measurement and calibration. The target is to reduce the proximity related influence to below 10  $\mu\text{A}/\text{A}$ .
3. Develop a precision voltage sensor for the calibration of non-conventional and conventional sensors in medium voltage networks. The target uncertainty for voltage measurement is below 100  $\mu\text{V}/\text{V}$  and the target bandwidth is 5 kHz.
4. Develop traceability for new non-conventional techniques not yet commercially available, such as using a fibre Bragg grating for interrogation of sensor networks, or measurement of capacitive current flow through a high voltage capacitor for PQ measurements. The target uncertainties are below 0.2 % and 0.3 crad.
5. Test the applicability of the sensors developed in the project on existing medium voltage (c. 20 kV) and/or high voltage (c. 100 kV) substations.
6. Develop services for the calibration of transformers and non-conventional sensors with analogue and digital output in line with IEC 61850-9-2

### 3 Research results

#### 3.1 Current sensor based on Faraday effect in optical fibre

Fibre Optic Current Sensors (FOCSs) are a class of compact and low cost sensors not affected by electric interference, and with potential to achieve a much higher bandwidth than conventional current measurement systems, i.e. up to tens of kilohertz rather than some kilohertz. FOCS are now relatively well established, being commercially available from a range of manufacturers, and offering compliance with the 0.1 or 0.2 metering and 5P or 5TPE protection accuracy classes. The technology allows DC and AC signals to be measured with the same device and the measured current levels of 600 kA, a repeatability of  $\pm 0.02\%$  and a temperature sensitivity of  $< \pm 0.002\%/^{\circ}\text{C}$  can be reached. The sampling rate for such systems is typically a few kS/s.

As the state-of-the-art FOCSs have 0.1 % and 0.2 % uncertainties, a traceable calibration method with a measurement uncertainty of 0.01 % is required for reliable calibration of such FOCSs.

The majority of commercial measurement systems work at 1310 nm or 1550 nm wavelengths because of the availability of off-the-shelf components. There are some examples of systems using 820 nm, which show better sensitivity than those systems operating at high wavelengths. Since the Faraday effect in a fibre, and its sensitivity, is approximately proportional to  $1/\lambda^2$ , an operating wavelength of around 650 nm was chosen to increase the sensitivity of the proposed FOCS even though availability of off-the-shelf components is limited. The use of new fibre materials, with rare earth doping to reduce shape-induced birefringence, was proposed to improve the existing systems further by utilising either spun or annealed fibres.

Three different optical signal detection schemes were studied. One was based on interferometric detection while the other two systems were based on phase sensitive detection. The final all fibre-optical system, which operates in the reflective mode configuration, was based on phase detection and was selected as best performing. A doped High Birefringence (HiBi) spun fibre was used as the sensing fibre to suppress the effect of birefringence.

##### 3.1.1 The Faraday effect

If a conductor is enclosed by an optical fibre, having a Verdet constant  $V$ , a full number of turns around a conductor with current  $I$ , a phase displacement of light in the fibre can be written as

$$\theta_f = V \oint B dl = \mu_0 V I \theta_f = V \oint B dl = \mu_0 V I,$$

where  $B$  is the magnetic field,  $\mu_0$  vacuum permeability, and  $\theta_f$  the rotation of the polarization angle due to Faraday effect.

In an optical fibre, the optical signal phase shift can be caused by the birefringence effect that can be either inherent or induced by fibre bending, and by the Faraday effect due to the existence of external electromagnetic fields around the fibre. These effects occur in a distributed manner, which brings a need to control the different contributions in order to detect only the Faraday effect, required for the current measurement purposes. One solution is to use birefringent material and spin the fibre. In this way, the sensitivity can be tailored for different length scales for the birefringence beat length and the spin pitch. In short, a HiBi fibre is desirable in order not to be sensitive to external influence, e.g. bending, vibration and temperature changes, but the length scale corresponding to the spin should still be the shortest, to mitigate the birefringence induced by fibre bending.

The main challenges in designing a FOCS that meets the target measurement range and uncertainty is the selection of the sensor fibre material; it should have suitable wavelength, large enough response and it should be possible to manufacture. Furthermore, one has to select the method for the detection of the polarisation change induced by the Faraday effect in the presence of competing effects. These requirements further break down to a selection of subsystem components, and to identifying their short and long-term stability. Several FOCS make use of the Faraday effect in an appropriately modified commercial fibre gyroscope (a system used for measuring or maintaining orientation and angular velocity). In these setups, one or two phase modulators are used with a reflective single-mode fibre. The output signal is detected with a lock-in amplifier. A low birefringence fibre is typically used and the fibre is twisted to reduce bend-induced linear birefringence. Much effort has also been made to compensate for temperature effects. In this project, we studied interferometric and phase modulation approaches for the detection of the Faraday effect.

### 3.1.2 Fibre development

Un-doped fibres with three different spin pitches and symmetrical core were sourced for with dimensions optimised for single-mode operation at 650 nm for testing in the interferometer and the open-air phase modulating system.

A measurement setup was designed and built at LNE with support from RISE, for characterisation of the fibre characteristics at 633 nm. The Verdet constant of un-doped material was found to be  $(3.97 \pm 0.38)$  and  $(3.64 \pm 0.09)$  rad/(T·m) for a fibre with a spin pitch of 5 and 7 mm. A Verdet constant of 2.11 rad/(T·m) at 820 nm has been reported in literature, which can be scaled to 3.54 rad/(T·m) @ 632.8 nm by the approximation that the Verdet constant follows  $1/\lambda^2$ . Overview of fibre characterization measurements is shown in Table 1. Comparing with the values within this work, the inverse square relation seems to hold.

Table 1: Overview of fibre characterization measurements (T=22.5 °C,  $\lambda=632.8$  nm).

Measurements	Type of optical fiber	V [rad/(T·m)]	V (sdev) [rad/(T·m)]	Comments
Sep – Oct 2015	Spun LoBi undoped 5 mm spin pitch	3.97	0.38	$\frac{dV}{dt} \cdot \frac{1}{V_0} = 1.2 \cdot 10^{-3} \text{ K}^{-1}$
Nov 2015	Spun LoBi undoped 7 mm spin pitch	4.50	0.09	
Jun 2016	Unspun, TbAl doped HiBi	2.0*	-	Very thin fibres. Cut-off wavelength 430 nm. Birefringence obscure the Faraday Effect.
Nov – Dec 2016	Spun TbAl doped 5 mm spin pitch	4.10	0.08	.
	Spun TbAl doped 7 mm spin pitch	3.94	0.55	

The temperature coefficient of the Verdet constant was measured for un-doped material and found to be  $1.2 \cdot 10^{-3} \text{ K}^{-1}$ . This value is higher than the  $1.2 \cdot 10^{-4} \text{ K}^{-1}$  reported elsewhere. However, the difference might be explained by the latent circular birefringence characterizing the spun fibres. When designing the FOCS, the variation of the Verdet constant with the temperature was considered and compensated.

Doping was done using Tb in  $\text{Al}_2\text{O}_3\text{-SiO}_2$  glass host. The material was spun and analysed. A Verdet constant of  $(4.10 \pm 0.08)$  and  $(3.94 \pm 0.55)$  rad/(T·m) was determined for a fibre with a spin pitch of 5 and 7 mm respectively. This is marginal improvement from an undoped fibre possibly owing to an absorption peak close to 633 nm.

The final step was to develop a spun HiBi (high birefringence) polarisation maintaining fibre. However manufacturing such a fibre was not successful during the lifetime of the project.

### 3.1.3 Testing of the interferometric system

A commercial interferometer, developed for length measurements, was tested. The signals of the system were sampled at 100 kS/s, which gave 20000 samples per period at power frequency. The sensitivity to phase change of this system is 0.3 mrad. A loop of 10 turns of LoBi (low birefringence) spun fibre was used in testing this system. The interferometer was originally designed for precise distance measurements, which means that it is also very sensitive to length changes. Unfortunately, the system proved to be very sensitive to acoustics and temperature changes, and a mechanical drift was observed. Moreover, during the experiment, temperature effects were observed as a slow drift in the phase displacement. Hence, a decision was made to focus on detection by phase modulation.

### 3.1.4 Theory and modelling of the phase modulation system

Theoretical study of propagation of light in sensor fibre was carried out by Chalmers University of Technology. The work produced a set of formulae describing in detail the performance of a system, where phase modulation is used together with a spun fibre for current detection. The block diagram of the system is shown in Figure 1. A Jones matrix representation was developed for the system, and it was used as a basis for creating a software for simulation of the sensor system. A screen capture of the simulator interface is shown in Figure 2.

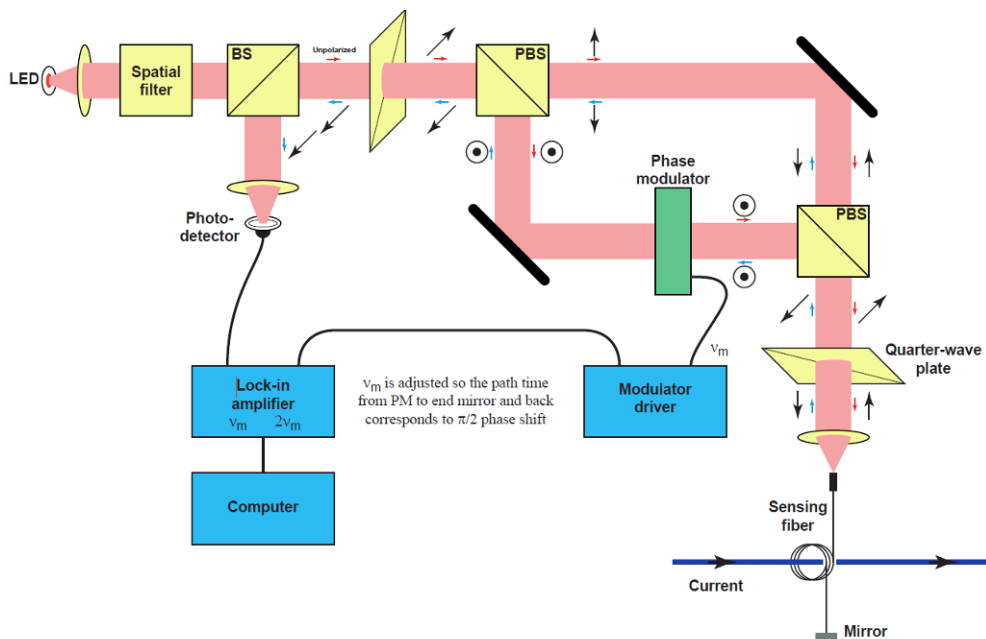


Figure 1: Block diagram of the phase modulation based designs of FOCS.

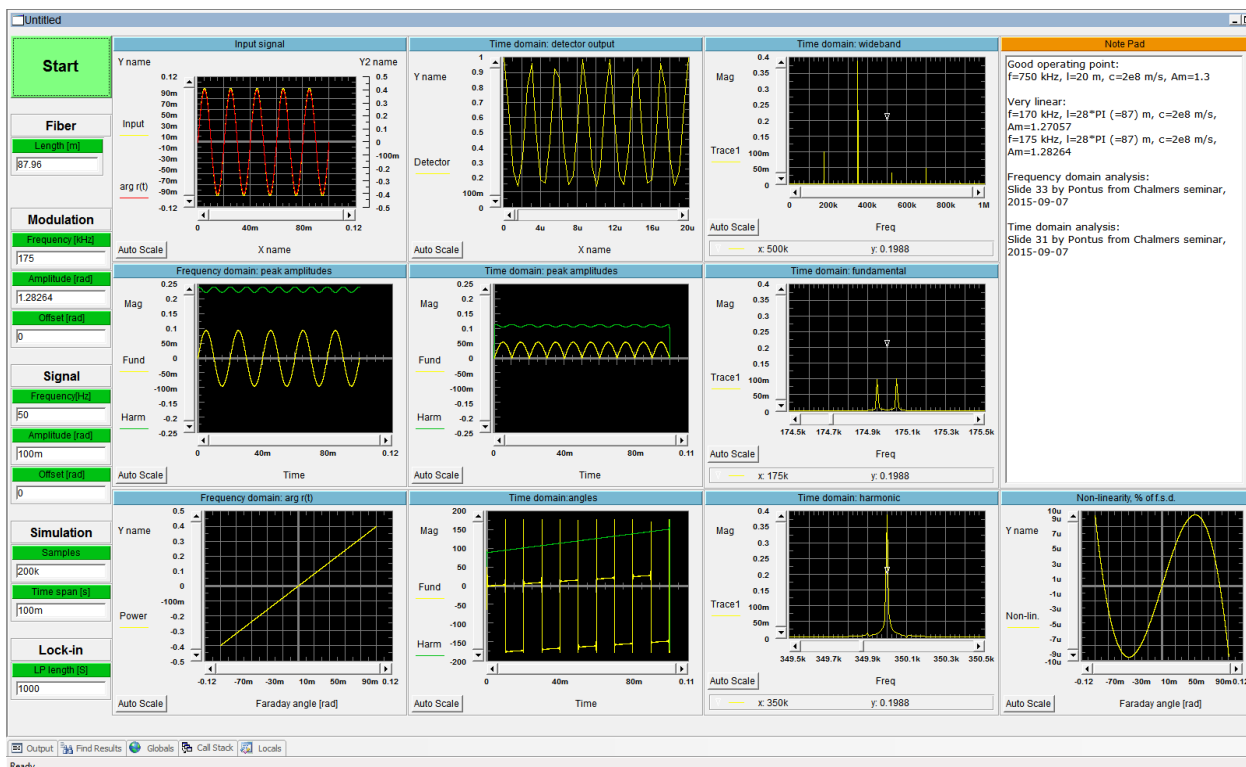


Figure 2: User interface of the FOCS simulation software.

**3.1.5 Phase modulation designs: open-air and all- fibre systems**

For the open-air system, high quality optical components optimised for operation around 650 nm were available off-the-shelf. A superluminescent diode source running at 650 nm was selected as source to avoid linewidth interference that is present when using laser diodes. The constructed system is shown in Figure 3. The sensor fibre is wound around the 1 m diameter ring white ring.

The design of the open-air system was a joint effort between VTT, RISE, LNE and University of Strathclyde. A researcher from VTT spent three one-week visits to SP between October 2016 and March 2017 to join them for development of readout systems and for system characterization measurements.

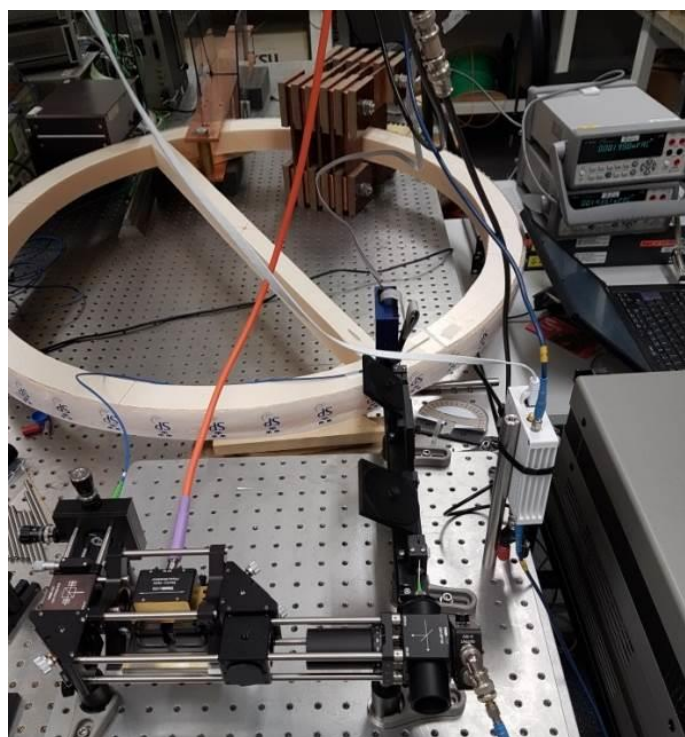


Figure 3: All optical components of the open-air system are in the foreground, white ring supports the detection fibre, and the coil for feeding the electric current is in the background.

The requirements on thermal and mechanical stability are very high, and the open-air design (Figure 3) has limitations but it has proven to work well in a laboratory set-up.

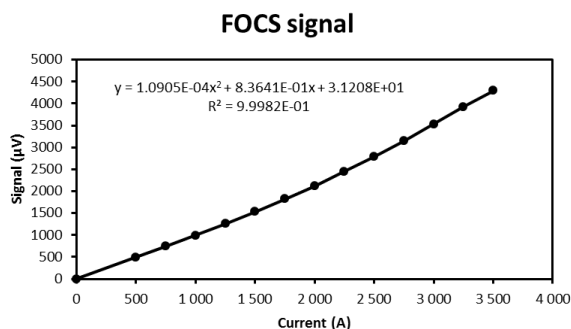


Figure 4: Open-air system response showing its linearity.

The response of the system running in open loop mode has been plotted in Figure 4, and the signal to-noise is better than 60 dB in detecting the magnetic field from currents above 500 A. The system response in the

tested open loop mode of operation is not linear. Because of this, preparations were started to run the system in closed loop mode to compensate for the inherently non-linear operation of the system.

The experiments on the open-air prototype showed that the system was sensitive to vibrations, acoustic coupling and temperature changes even at stable laboratory conditions. An all-fibre system shown in Figure 5 was designed and built to overcome these problems. Unfortunately, obtaining suitable fibres to reach the targets was more difficult than anticipated so only shorter wavelength (650 nm) operation was demonstrated with the setup.

The objective was to perform on-site calibrations with an uncertainty below 100  $\mu\text{A/A}$  (0.01 %). However, the uncertainty demonstrated by the end of the project was 1 % in the range from 400 A to 3500 A, in laboratory conditions. The full capability of the new design could not be fully explored during the project.

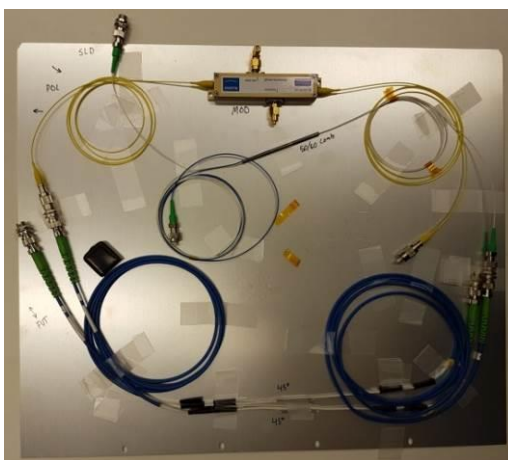


Figure 5: Assembled all-fibre system.

### 3.1.6 Conclusion

A concept has been developed for producing HiBi (High Birefringence) spun fibre, which is crucial for the current detection. Doping of fibre material to increase the response was not successful, probably owing to absorption of the dopant. The interferometer design offered highly sensitive detection, but was sensitive to perturbations as acoustics and temperature. The phase detection design chosen provided a robust and sensitive solution but it needs further development before it can be used for metrology and possible future on-site calibration. In parallel to the experimental work, a software implementing the theoretical model of the complete system is now available. The model can be used for further optimisation of the developed FOCS.

## 3.2 Magnetic shielding technique for a Rogowski coil

Output voltage of a Rogowski coil is proportional to the coil's mutual inductance,  $M$ , and to the derivative of current ( $di / dt$ ),

$$u = M \frac{di}{dt}.$$

Induced voltage caused by the magnetic field should be integrated in order to have the waveform representing the original current flowing through the coil. If the voltage is not integrated, the output voltage is depending linearly on frequency. Voltage signal is increasing in direct proportion with increasing frequency. Rogowski coil has no ferromagnetic material in the core and thus the coil cannot be saturated. This means that the device has an excellent linearity. The coil can be calibrated at low current, with few amperes, and it can be used for high current measurements.

The Rogowski is assembled around medium or high voltage conductor, which acts as the primary winding of the coil. The secondary winding of the Rogowski coil is uniformly wound on a non-magnetic core and electrostatically shielded, as usual. The solution studied in this project adds a magnetic shield around it. The

magnetic shield is constructed as a hollow toroid enclosing the Rogowski Coil. The shield consists of two high permeability tape-wound toroidal magnetic cores and two flat rings of mu-metal. Insulation sheets are used in the assembly of the magnetic shield to prevent the formation of a short circuit. The cut-away view of magnetic shielded Rogowski coil is shown in Figure 6.

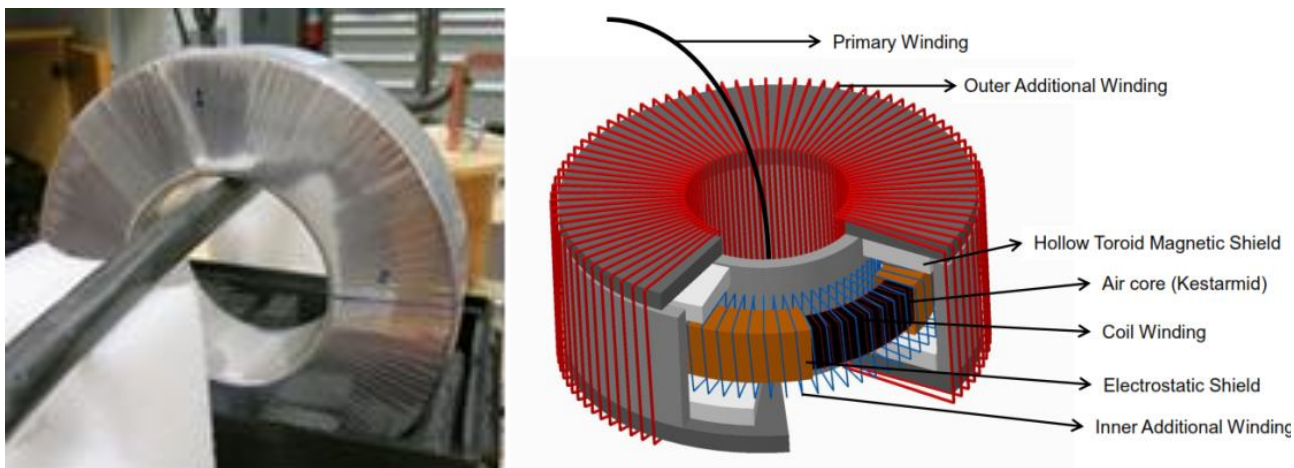


Figure 6: Left: The magnetically shielded Rogowski coil. Right: Cut-away view of the coil.

To avoid the saturation of the magnetic shield, two additional windings are installed inside and outside the hollow toroid. These windings, having the same number of turns (400), are connected to each other in series but inversely so that their ampere-turns cancel each other. The magnetic shield does not change the mutual inductance of the Rogowski Coil, but it prevents the influence of unwanted magnetic fields. The principle of magnetic shielding is similar to that used in current comparators.

In a Rogowski coil, two main factors change with rising temperature:

- The coil former expands, thus increasing the effective area of the winding and sensitivity of the coil, and
- The resistance of the copper wire increases. This reduces the sensitivity of the coil by a factor, which depends also on the load resistance of the coil.

These two effects can be made to compensate each other by connecting a suitable stable resistor in parallel with the output of the coil. Typical temperature coefficient of an uncompensated coil is c. 50 ppm/K. Compensation can reduce this by more than one order of magnitude.

The measured mutual inductance and the phase displacement on frequencies from 50 Hz to 60 Hz are shown in Table 2. Signal to noise ratio is slightly worse at 50 Hz, but results on 53 Hz to 60 Hz agree well.

Table 2: Calibrated mutual inductance and phase displacement, and their uncertainties ( $k = 2$ ), as function of frequency.

Frequency [Hz]	Mutual inductance [nH]	Phase displacement Difference from $\pi/2$ [crad]
50	3563.23 ± 0.06	0.035 ± 0.002
53	3563.22 ± 0.04	0.037 ± 0.002
55	3563.21 ± 0.04	0.038 ± 0.002
60	3563.21 ± 0.04	0.041 ± 0.002

Due to its large mass, the coil responds to changes in temperature slowly. The estimate time constant is about three hours. Temperature dependency measurement was performed with several load resistance values connected in parallel with output of the coil, in order to find the value that leads to the lowest temperature dependence. In this case, the optimal resistance value was 9.5 kΩ. Figure 7 shows the dependence of mutual inductance with the optimal temperature compensation.

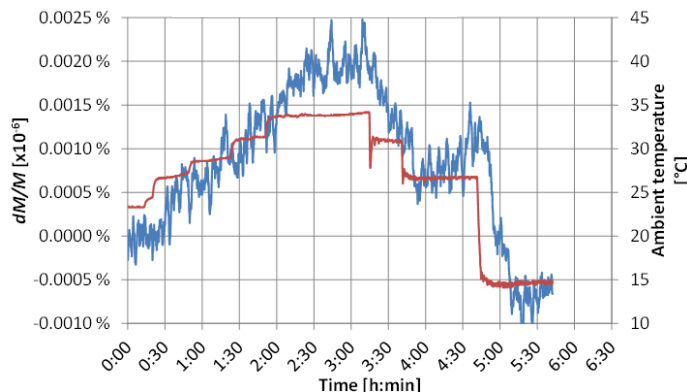


Figure 7: Temperature dependence of the mutual inductance with temperature compensation. Red curve: temperature, Blue curve: mutual inductance.

The linearity of the coil was checked up to 600 A against a reference Rogowski coil, as shown in Figure 8. The measurement was performed with 60 Hz current for the temperature compensated coil.

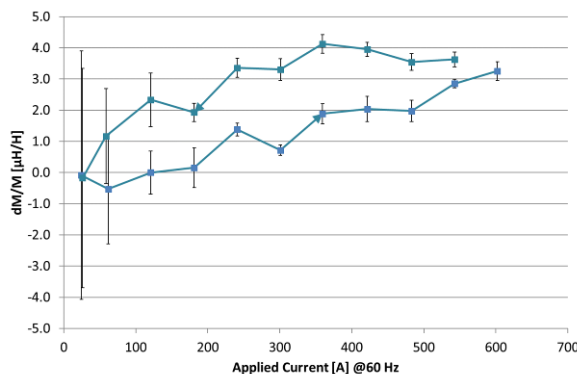


Figure 8: Current linearity check. Readings obtained when rising voltage (lower curve) and lowering voltage (upper curve) are shown. The error bars show one standard deviation of the results.

Position dependence measurements were performed on currents from 60 A to 80 A, on 55 Hz frequency to the temperature compensated coil. First, the influence of the conductor position in the coil was studied. A conductor with 20 mm diameter was fed once through the coil. The setup is shown in Figure 9. The reference value was measured when the conductor was fed through the centre of the coil. Then the conductor was moved to four directions, until it touched the coil. Results of the measured position dependence are given in Table 3.

Similar exercise was repeated to study how the closeness of return conductor interferes with the measured current. The position of the return conductor with 20 mm diameter was changed. The setup is shown in Figure 10. The reference value was measured when the return conductor was 80 cm from the centre of the coil. Then the distance was varied for 20 cm (touching the coil) to c. 130 cm. Results of the measured return conductor distance dependence are given in Table 4.

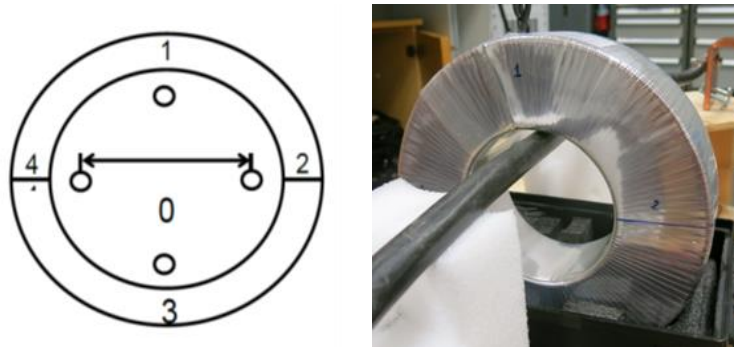


Figure 9: Setup for measuring of sensitivity to feeding conductor position.

Table 3: Effect of feeding conductor position on mutual inductance and phase displacement.

Position No:	Mutual inductance		Phase displacement	
	[ $\mu\text{H}/\text{H}$ ]	St.dev. [ $\mu\text{H}/\text{H}$ ]	[ $\mu\text{rad}$ ]	St.dev. [ $\mu\text{rad}$ ]
0	0.0	0.4	0.0	0.3
1	2.6	0.6	-0.2	0.5
2	1.6	0.5	-1.2	0.7
3	-0.8	0.4	-1.3	0.8
4	-1.2	0.6	-0.3	0.6

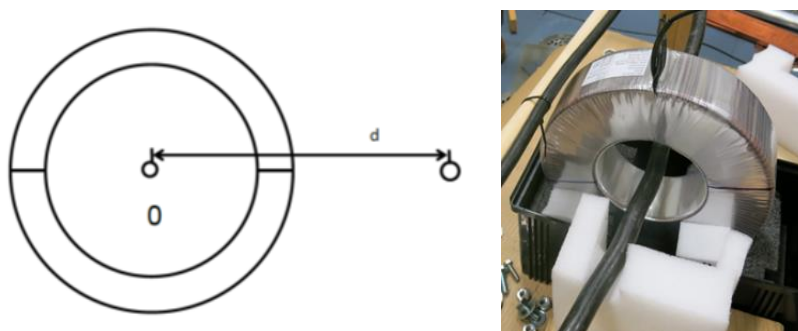


Figure 10: Setup for measuring of sensitivity to return conductor position.

Table 4: Effect of return conductor distance on mutual inductance and phase displacement.

Distance d [cm]	Mutual inductance		Phase displacement	
	[ $\mu\text{H}/\text{H}$ ]	St.dev. [ $\mu\text{H}/\text{H}$ ]	[ $\mu\text{rad}$ ]	St.dev. [ $\mu\text{rad}$ ]
21	-5.5	4.4	-1.6	8.3
40	-1.2	2.9	-1.9	4.9
60	0.1	2.4	-1.2	3.1
80	0.0	2.6	0.0	4.0
98	-1.9	0.9	0.6	10.3
127	-0.6	0.9	-1.2	4.7

The results shown in Table 3 and Table 4 mean that the position of the primary conductor does not have influence to the uncertainty of measurement even for the most demanding on-site calibrations.

The testing of the Rogowski coil prototype was a joint effort, where VTT was responsible for low voltage, TUBITAK for medium voltage, and FFII for high voltage measurements.

### 3.3 Precision voltage sensor for medium voltage networks

The most important advantage of voltage dividers over traditional voltage transformers is that voltage dividers do not have an iron core with non-linear hysteresis characteristics. Voltage dividers have linear behaviour with respect to over-voltages and a flat frequency response from DC to high frequency range. The weak point of a voltage divider is the influence of external high voltages and earth parts in its vicinity. Electrical fields arising from high voltages in neighbouring phases and from ground conductors and structures are one of their main sources for systematic measurement errors. A shielded voltage divider for 24 kV medium voltage network was designed and insulated in SF<sub>6</sub> gas composed by two resistive-capacitive dividers, achieving a flat frequency response up to 10 kHz for ratio error and up to 5 kHz for phase displacement error. The metal shielding improves its immunity against electric and magnetic fields. The characterization performed on the built-in voltage sensor shows an accuracy class of 0.2 for a frequency range from 20 Hz to 5 kHz and class of 0.5 for DC up to 20 Hz. A low temperature effect is also achieved for operation conditions of MV power grids.

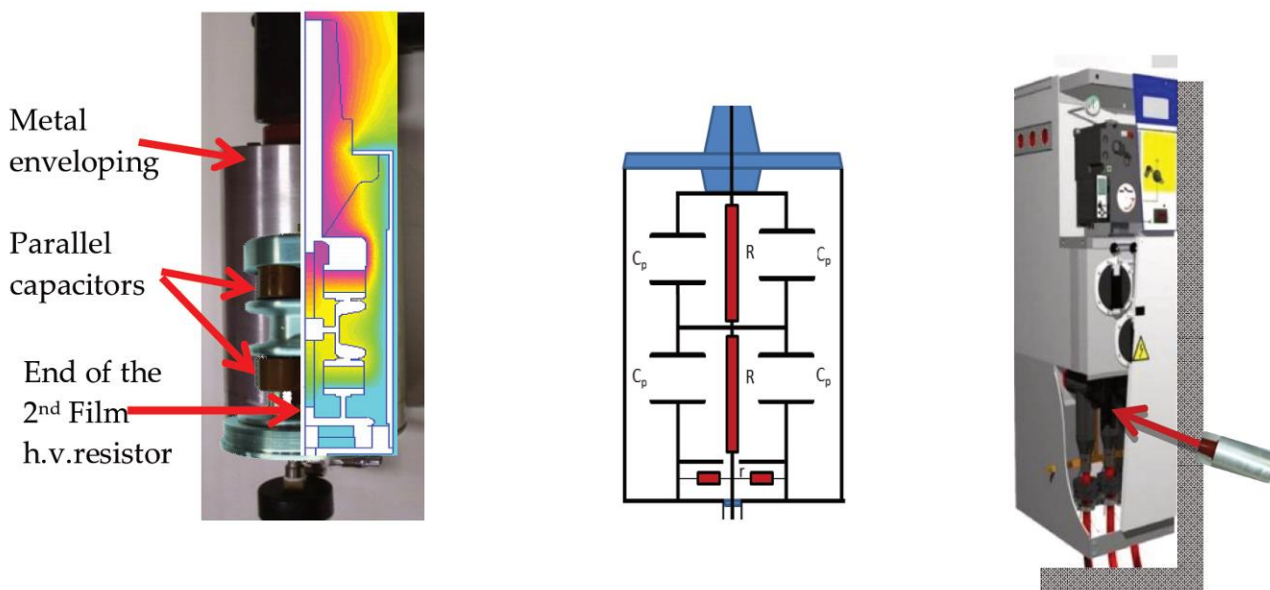


Figure 11: Resistive voltage probe for medium voltage switchgear. Left: cut-away view of the voltage probe. Centre: Schematic diagram of the probe. Right: Typical switchgear and the probe.

The voltage divider consists of a 50 MΩ high voltage resistive branch, composed of two h.v. film resistors,  $R$ , of 25 MΩ connected in series, as shown in Figure 11. The low-voltage resistive branch of the divider,  $r$ , of 50 kΩ is composed of four 200-kΩ resistors arranged in parallel in a coaxial configuration, in order to reduce the inductive effect. Two blocks of four capacitors of 202 pF each form two capacitances,  $C_p$ , of 808 pF, which are connected in series, surrounding each high-voltage resistor. The first block of capacitors is connected in parallel with the first resistor of the high voltage branch through an upper electrode and a central electrode. The second block of capacitors is connected between the central electrode and the enveloping. The central electrode serves as mechanical support for the two capacitor blocks, and for the two resistors of the high voltage branch. The configuration is designed to achieve a voltage distribution along each h.v. resistor for higher frequencies as close as possible to the voltage distribution obtained for 50 Hz. The voltage distribution along the h.v. resistors was determined by FEM simulation for the frequency range from 50 Hz to 5 kHz (see Figure 12). The central electrode, midpoint of the high voltage resistances, is at half potential of the voltage

input. The set is in a steel-aluminum casing to achieve a good electrical and magnetic shielding. The low voltage branch is also arranged in an aluminum compartment, different to the high voltage branch, although sharing the same gas insulation. SF<sub>6</sub> gas at 0.2 MPa is used as internal insulation in order to pass dielectric tests corresponding to the insulation level of 24 kV. A plug-in connector is used to connect to the cable entry of the enclosed metal box.

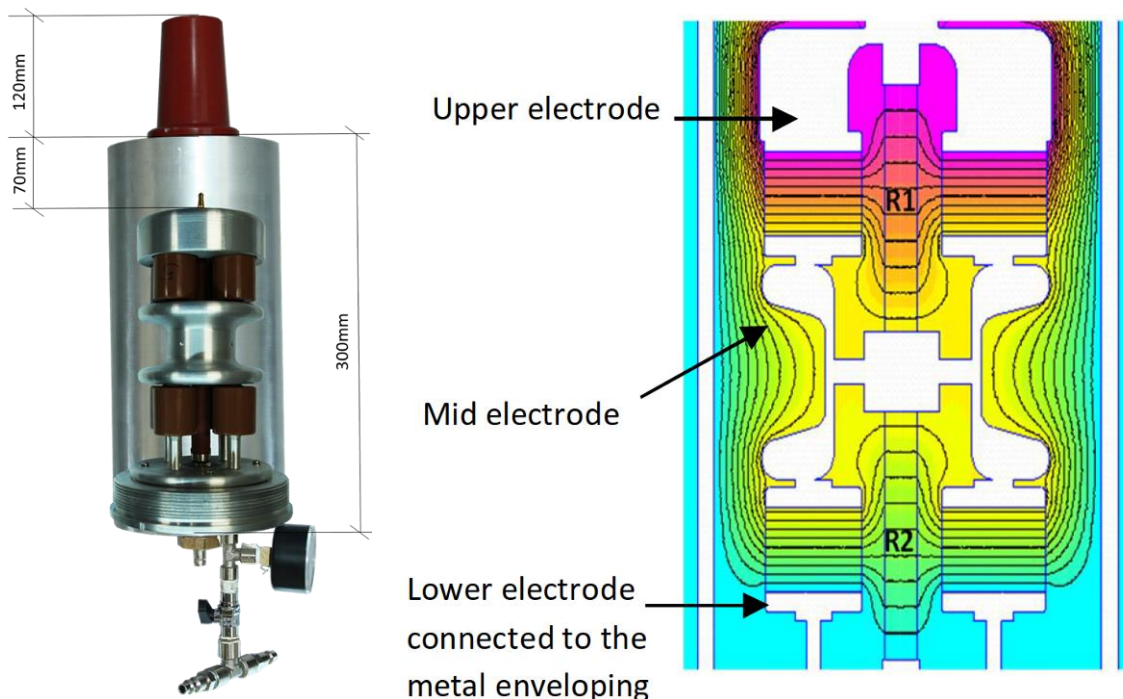


Figure 12: Resistive voltage probe for medium voltage switchgear. Left: dimensions. Right: Simulated electrical field distribution.

Two circuit models were made for simulation of the frequency response of the design (see Figure 13). The simplified model did not explain the measured response of the prototypes in enough detail, and an improved version was made to support to the design of the final version of the voltage probe. Comparison between the measured frequency response of the probe and the two models is shown in Figure 14.

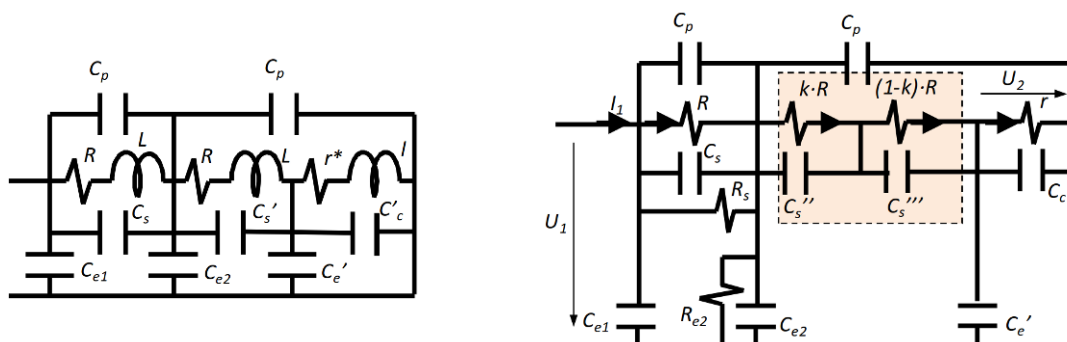


Figure 13: The two electrical models used for simulation of the probe frequency response. Left: Simplified model. Right: Improved model.

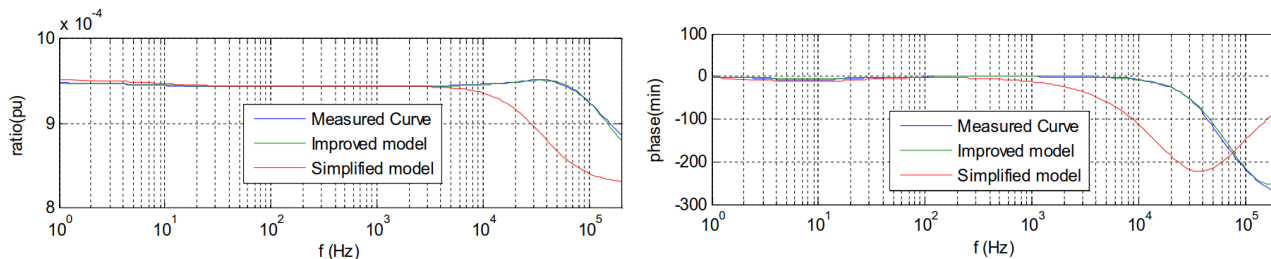


Figure 14: Comparison between theoretical and measured frequency responses of the voltage probe.

### 3.4 New non-conventional sensor techniques

#### 3.4.1 Current clamp

The aim of this work was to develop a new method for the measurement of voltage harmonics and associated power quality on medium and high voltage lines by measuring the current through an already installed capacitor in the grid. The arrangement of the measurement is shown schematically in Figure 15. It shows the simplified setup of the proposed current clamp based voltage-monitoring system (CCVM). The capacitor  $C_M$  is connected to the high voltage UHV (line to earth). The current  $I_M$  through the capacitor can be measured using a current clamp at the grounded side of the capacitor. This has the advantage that the clamp can be connected during operation and without interrupting the high voltage. Thereby a lead cable, which is at earth potential, must not be opened.

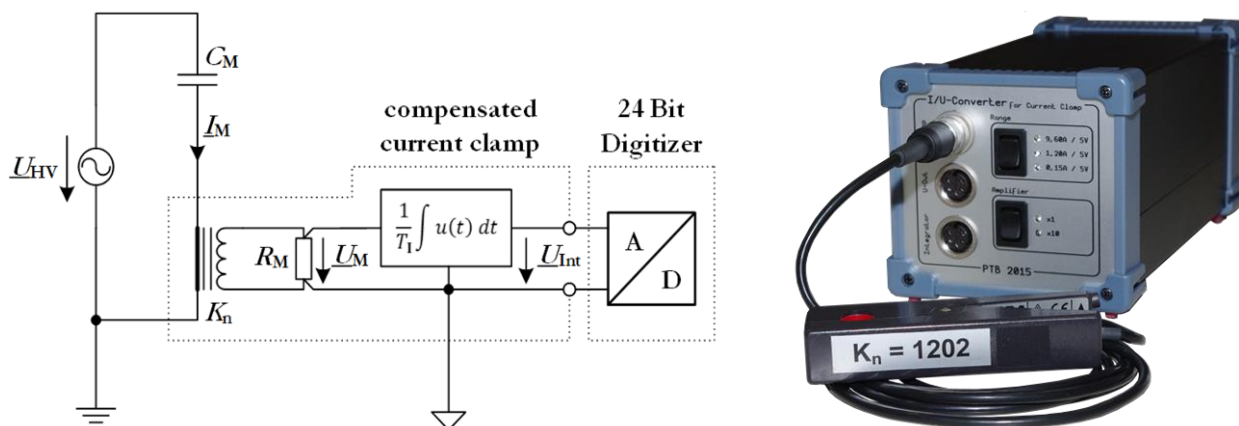


Figure 15: Current clamp based system for measurement of harmonics on medium and high voltage grids.

The presented CCVM including its current clamp sensor and the sampling system was initially verified for correct and accurate operation in a period of around five days. For that purpose a calibrated capacitor (WIMA MKS4) with  $C_M = 0.9212 \mu\text{F}$  and a  $\tan\delta = 1.25 \cdot 10^{-3}$  was connected to the 230 V / 50 Hz LV grid. The capacitive current of about 66 mA was measured in the 150 mA range of the sensor. A two-stage voltage transformer with a ratio of 240 V / 3 V and with an accuracy of  $10^{-5}$  was used to provide a reference voltage for the two-channel sampling system. Both voltages were measured applying a window width of 1 s. To limit the number of results in 5 days, a 30 s moving average of the voltage, frequency and the total harmonic distortion THD were calculated and stored. Using the results of these measurements, the accuracy of the root mean square (rms) value and the phase angle of the CCVM are calculated by comparison with output of a reference voltage transformer. These results are shown in Figure 16. The rms error (red curve) is in a range below 0.05 %. The drift is explained by small temperature changes during the measurements and the relatively high temperature coefficient (0.03 % / °C) of the capacitor. After correcting the measured values by using the  $\tan\delta$  of the capacitor, the phase displacement of the CCVM is smaller than 0.05 crad and without any visible drift.

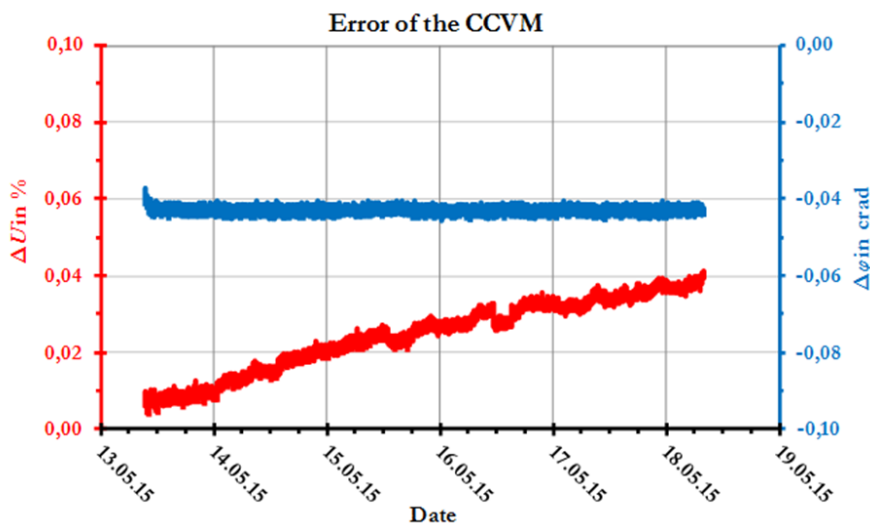


Figure 16: Accuracy of the CCVM in a time interval of 5 days.

The proposed method and the current clamp-based sensor demonstrates the feasibility of monitoring high voltage harmonics by measurement of current through a capacitor already installed in power grid. Considering that the achieved accuracy of the sensor was better than 0.1 %, the limitation of the accuracy of the determined high voltage parameters (rms value, and phase angle) is the uncertainty of the parameters of the used capacitor ( $C, \tan \delta$ ). If a high-quality HV capacitor is available, accurate measurements within 0.5 % for rms values and phase angle are possible in the HV grid. Such accuracies are usually more than adequate for monitoring purposes.

In the future, the measuring capabilities of the CCVM will be improved with better software and more algorithms, adapting the needs for comfortable on-site measurements. Furthermore, the CCVM will be tested at different locations in the LV and MV grid. Development and testing of current clamp measurement system was a joint effort of PTB and TU Dresden.

### 3.4.2 Interrogation using fibre Bragg grating

Three key elements comprise the optically interrogated current sensor (OCS): i) a primary current transformer (CT), ii) a PCB containing a burden resistor and protection components (to protect against the effects of over-voltages on the inputs to the sensor), iii) and the Low Voltage Transducer (LVT). In this project, main emphasis was put on using a conventional current transformer as transducer.

In Figure 17, a cut-away CAD drawing of the transducer is presented. The elements inside the package include the optical fibre with the fibre-Bragg-grating (FBG), the piezoelectric actuator with two ceramic end caps, and two Kovar pins, which provide the electrical connection to the piezoelectric actuator and form electrical terminals outside of the device.

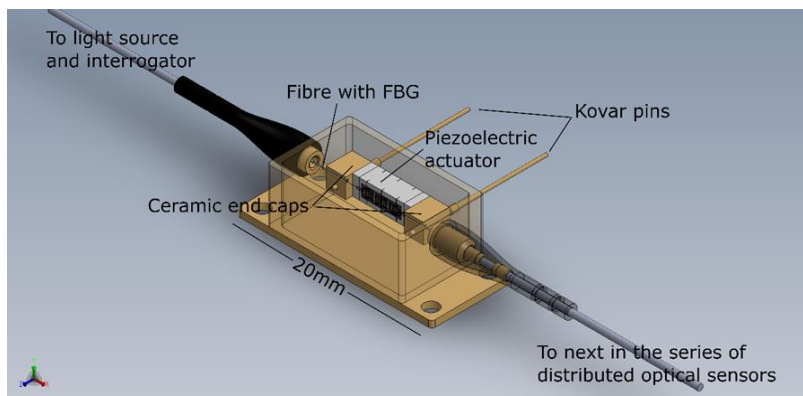


Figure 17: Low Voltage Transducer (LVT) with fibre Bragg grating

Figure 18 (a) shows the schematic diagram of the circuit that interfaces the current transformer secondary with the LVT. This includes the burden resistor  $R_b$ , the protection resistor  $R_p$  and the transient voltage suppression (TVS) diode. The constructed PCB board is shown in Figure 18 (b). It can be seen that the LVT is slightly smaller than the burden resistor.

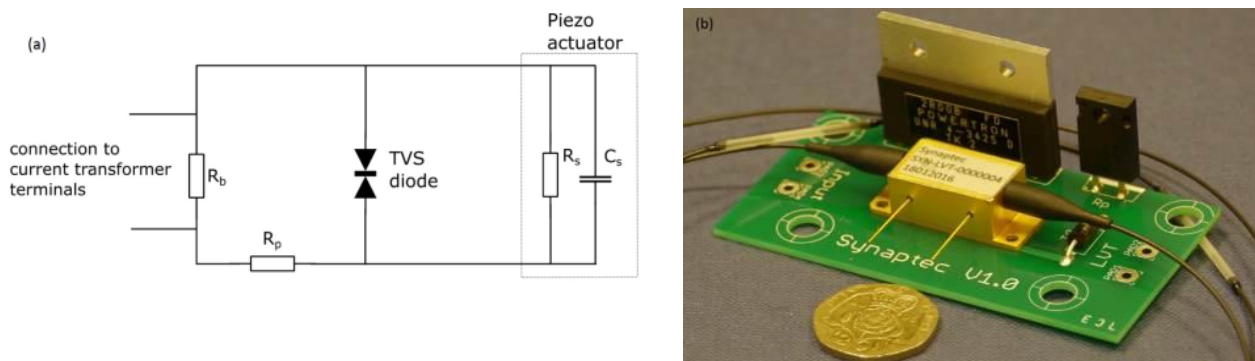


Figure 18: Electrical read-out and protection circuit for current transformer (a) schematic and (b) manufactured PCB.

Figure 19 shows the exterior view of the optical voltage transformer. The transducer is mounted inside a 400 mm long, hollow-core glass fibre insulator, which is rated to withstand a peak voltage of 75 kV. The hollow core insulator is sealed at bottom and top by a pair of flange plates, with the bottom plate doubling as a modular mounting bracket. A modular line connector is mounted on the top flange plate. The bottom flange plate is attached to a mounting plate, which has been appropriately sized for the requirements of the Power Networks Demonstration Centre (PNDC) test site at University of Strathclyde. The mounting plate is earthed through an M16 copper stud.

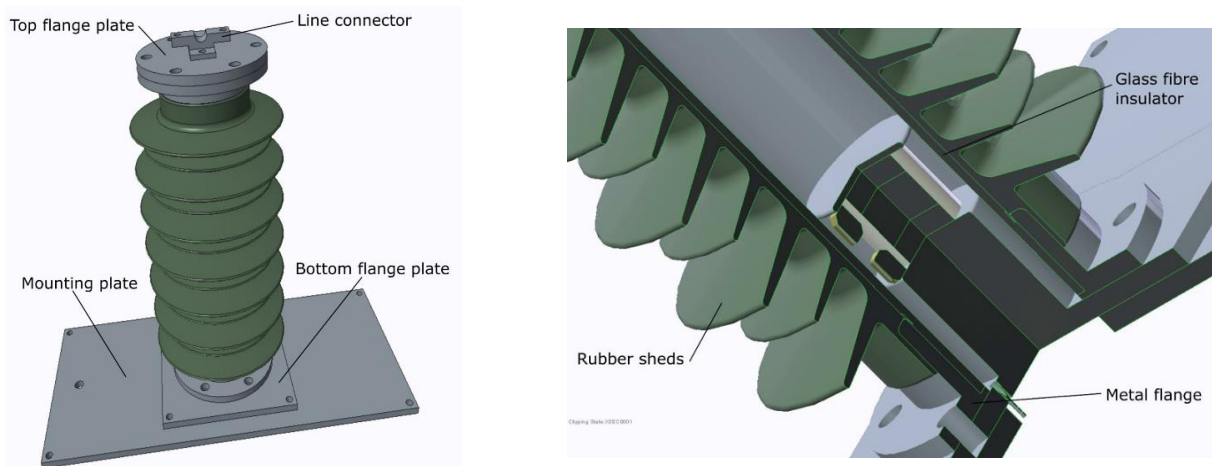


Figure 19: Left: CAD drawing of an exterior view of an Optical Voltage Transducer. Right: Cutaway view of the Optical Voltage Transducer

The transducer itself is shown in more detail in Figure 20. The insulator and rubber sheds are not shown for clarity. The upper electrode is connected to the line connector at the top flange by a 15 mm<sup>2</sup> cable, also not shown. The lower electrode is connected directly to the bottom flange plate, which is earthed. A fibre which contains a fibre Bragg grating (FBG) is epoxied (using EPO-TEK® 353ND) between the two shaped quartz pieces which form the strain-amplifying bridge. These are in turn epoxied to the upper and lower electrodes.

A piezoelectric transducer, a cylinder of PIC181, 40 mm diameter, and 40 mm in length, is epoxied between the two electrodes. When a voltage is applied to the line connector, it creates a potential difference between the upper and lower electrodes, causing an extension or contraction of the piezoelectric transducer. The lower electrode is fixed, so the upper electrode is forced to move. This causes a strain in the fibre attached to both

electrodes through the strain amplifying bridge. This leads to a change in the reflected wavelength of the FBG, which can be detected by an FBG interrogator; this wavelength change can then be used to reconstruct the line voltage waveform.

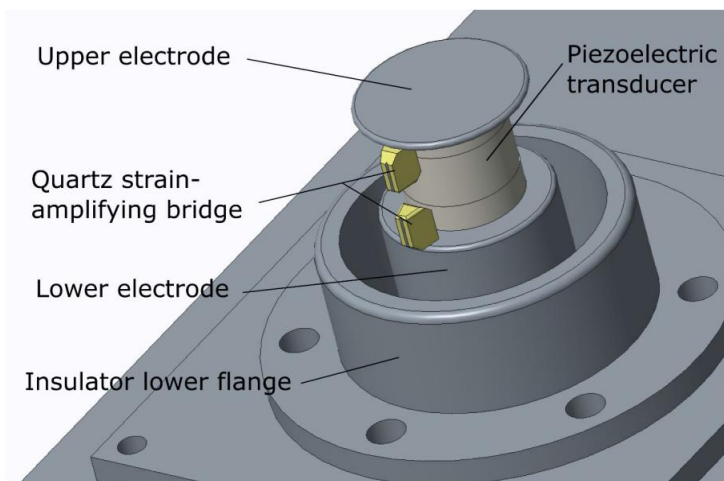


Figure 20: Left: CAD drawing of an exterior view of an Optical Voltage Transducer. Right: Cutaway view of the Optical Voltage Transducer

Characterization of the prototype voltage and current sensors shown in Figure 21 was performed at VTT during a visit of researcher from University of Strathclyde.



Figure 21: Transducers using fiber Bragg grating for readout. Left: 11 kV voltage transformer. Right: 1.2 kA split core current transformer

### 3.5 Testing of the developed sensors

#### 3.5.1 Laboratory testing of the developed Rogowski coil

The shielded Rogowski coil developed for objective 2 was used for on-site calibration of a medium voltage current transformer. The calibration was performed by applying appropriate primary current both to the current transformer to be calibrated, and to the Rogowski coil. The ratio error and phase displacement of the current transformer (CT) under test was determined using a bridge for non-conventional current transformers. The measuring arrangement is shown in Figure 22.

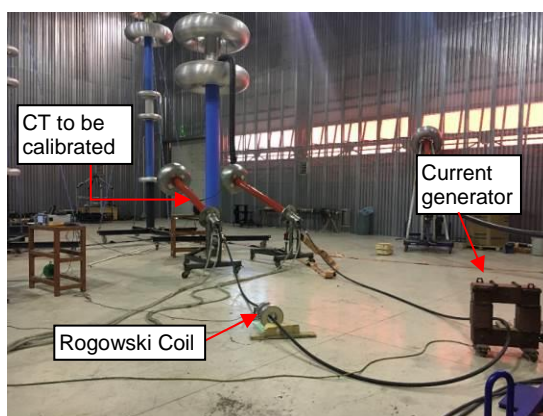


Figure 22: On-site calibration of current transformers using the Rogowski coil.

The effects of the magnetic coupling were less than 10 ppm by applying magnetic shielding to the coil. The temperature dependence of the shielded Rogowski coil was less than 5 ppm (18°C - 21 °C) with the 9.5 kΩ resistor connected to its output for temperature compensation.

The uncertainty budget of the measurement system is given in Table 5. Contributions of both type A (repeatability,  $N = 10$  measurements) and type B (calibration of the coil, the bridge, effects of magnetic coupling, linearity and influences of temperature change) uncertainties are included.

Table 5: Uncertainty Budget

Uncertainty Sources	Ratio ( $\mu\text{A/A}$ )	Phase ( $\mu\text{rad}$ )
Shielded Rogowski Coil	20	20
WM3000I (ECT Part)	80	70
Linearity	5	5
Effect of conductor position	5	2
Effect of external magnetic field	10	3
Ambient Temperature	5	5
Repeatability	20	30
<b>Expanded Uncertainty</b>	<b>100</b>	<b>100</b>

Uncertainties of 100  $\mu\text{A/A}$  for ratio and 100  $\mu\text{rad}$  rad for phase displacement were achieved with this method onsite.

Comparison of the coil in a high voltage setup against a reference CT was also performed. Figure 23 shows the setup at FFII, Spain. The setup is built on a trailer for on-site calibration of energy measurement systems. The Rogowski coil was connected on the same conductor with the CT shown in red.

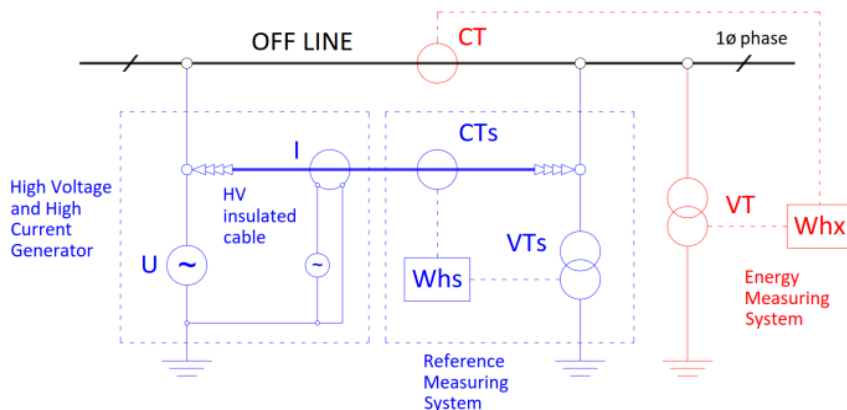


Figure 23: Setup for the high voltage comparison between the developed Rogowski coil and traditional calibration system. Blue: mobile setup, red: system under calibration, black: HV line.

This on-site measuring method is to keep the system under calibration connected to the three-phase voltage while current is applied by the mobile setup through one of the phases, which allows simulating conditions very similar to those of real operation. The secondary of the standard voltage transformer and standard current transformer supply the high voltage and high current generators. The HV cable already present in the system will provide the insulation also for the Rogowski coil. Performance of the CT will be compared with that of the Rogowski coil.

### 3.5.2 Medium voltage testing of voltage probe

Before a component can be installed in power network, it has to pass a series of tests to show that its insulation can withstand specified overvoltages. The insulation tests were usefully passed corresponding to the insulation level for material to be used in a power grid of 24 kV. Fifteen positive and negative lightning impulses 1.2/50 of 125 kV were applied without breakdown and a power frequency voltage of 50 kV ( $U_{peak}/\sqrt{2}$ ) for one minute was applied, also without breakdown.

The tested resistive divider was connected directly in the medium voltage grid in real operating conditions in the High Voltage laboratory of FFII (see Figure 24). Measurement errors and uncertainties are within the class 0.2 for both 50 Hz and 60 Hz in a wide range of voltages. The divider complies with the requirements set for voltage transformers where the ratio error shall be less than 0.2 % and the phase displacement error less than 10 minutes. The ratio error and phase displacement error corresponding fulfil requirements for class 0.2 from DC to 5 kHz range to be used in power grids up to 24 kV.



Figure 24: The voltage probe connected to medium voltage switchgear during ac test.

### 3.5.3 Medium voltage testing of the current clamp

The measurement was performed in a medium voltage (MV) substation at Dresden University of Technology. Table 6 shows the conditions of the measurement and the parameters of the MV cable.

Table 6: Conditions and parameters of the measurement.

Condition/Parameter	Value
Nominal voltage of the MV grid	20 kV
Type of MV cable	N2XS(F)2Y 1x150/25
Length of the MV cable	approx. 40 m
Load of the MV cable	None (idle at cable end)

The current clamp was installed in the shield to earth conduction of the MV cable (phase L2). Figure 25 schematically shows the measuring setup, and the connection around cable grounding wire is shown in Figure 26. In addition to the shield to earth current, the line to earth voltage was measured by using an already installed voltage transformer.

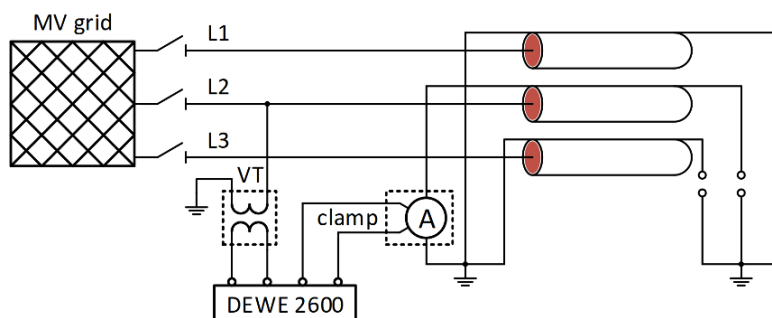


Figure 25: Current clamp connection to one phase of medium voltage installation.



Figure 26: Current clamp connected around medium voltage cable wire.

The output voltage of the current clamp, as well as the secondary voltage of the VT were measured synchronously by using the data acquisition system DEWE-2600. For the measurements, a sample rate of 100 kHz was chosen and the cut-off frequency of the anti-aliasing filters (Butterworth characteristics) was set to 30 kHz.

While measuring the currents at the beginning of the cable, the shield to earth conduction at the end of the line has been open. Otherwise, the magnetic fields of nearby MV conductors would cause circulating currents in the shield of the cable. These currents would be much higher than the capacitive currents between the conductor of the cable and its shields and would overlay the desired measuring signal. Figure 27 shows the recorded levels of some higher harmonics recorded by the current clamp.

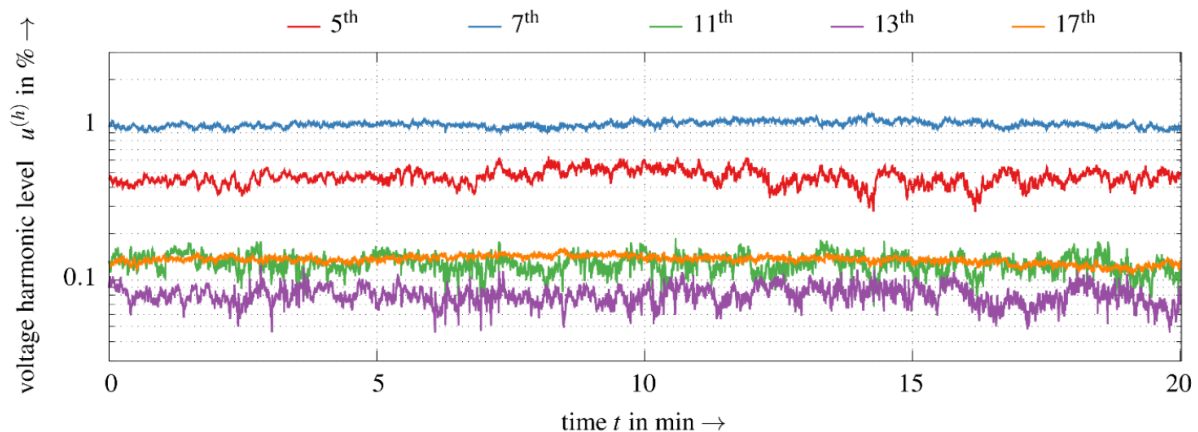


Figure 27: Voltage harmonics based on measurement by the capacitive current using the clamp.

The test measurements at the MV cable shows that the current clamp is generally suitable to measure the current in the shield to earth conduction of a MV cable. The voltage harmonics at this MV cable can be determined by evaluating the measured current flow.

However, this measurement method requires that the shield at the opposite side of the cable is not connected to the earth. Otherwise, circulating currents in the shield will prevent correct measurement.

### 3.5.4 Laboratory testing of the fibre Bragg grating based sensors

The two sub-elements of the optical current sensor – the conventional PX class current transformer and burden resistor, and the low voltage transducer – have been characterised separately and each has been found separately to meet the accuracy requirements of the IEC-60044-8 standards for the 5P and 5TPE protection classes.

The two sub-elements were also tested in combination as an optical current sensor (OCS) and found to meet the required accuracy standards for both amplitude and phase error. The optical current sensor has thus met all of the accuracy requirements for the 5P and 5TPE protection classes. Compensation for temperature, requiring time consuming calibration runs, has not yet been implemented and as a result, the temperature cycle accuracy test has not yet been carried out on the complete OCS device. The conventional CTs have marginal response to temperature in the required range, and the effect can in this case be ignored. However, the LVT shows a temperature response, which dominates even after it has been compensated for.

In conclusion, a rigorous testing scheme has been carried out on the optical current sensors, which have been found to meet the accuracy requirements of the IEC-60044-8 protection class standards.

One of the optical voltage transformers (OVTs) have been subjected to partial discharge testing by subjecting it to its power frequency withstand voltage of 28 kV for one minute and then observing the partial discharge level at  $U_m$  of 12 kV. No partial discharge larger than the 50 pC required by the standards was observed.

The same OVT has been tested against a reference device with 0.01 % uncertainty, in order to test its performance against the accuracy requirements of the measurement classes of EVT. Setup for the accuracy testing is shown in Figure 28. It was found that at steady state, and when there were no rapid voltage changes greater than 10 % of nominal, the OVT met the requirements of the 0.2 accuracy class. However, when rapid voltage changes of greater than 10 % occurred, the OVT could exhibit amplitude errors greater than the required 0.2 % for approximately 60 s. Furthermore, in the event of the OVT experiencing an overvoltage at the power withstand or lightning impulse levels, the amplitude error could increase to ~5 % for several hours.

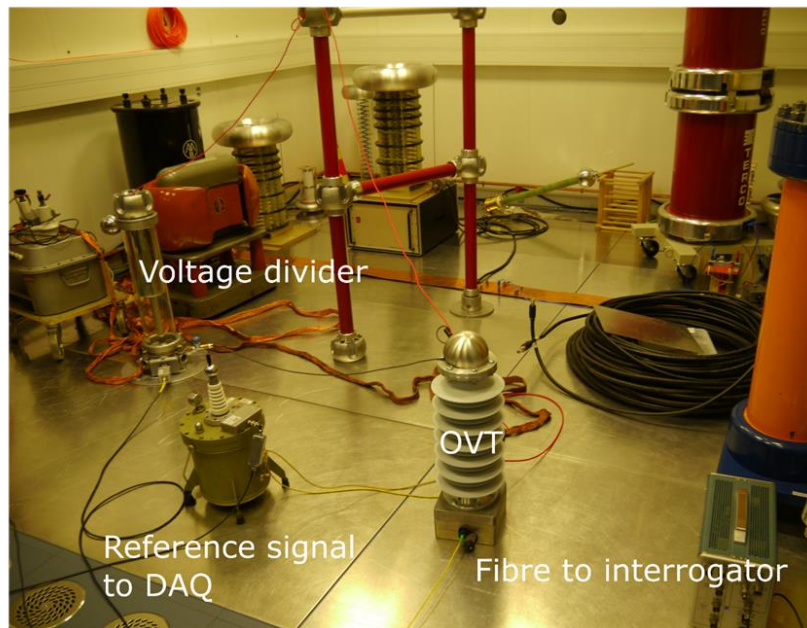


Figure 28: Setup for OVT accuracy testing at VTT.

The OVT has also been shown to meet the limits of the 3P protection class, with an amplitude error less than 0.5 % at 2 % of nominal voltage. The limit required by the standard is an amplitude error of 6 %. Switching rapidly from 2 % of nominal to 100 % of nominal did not cause the OVT to exceed the 3 % amplitude error requirement. However, the same caveats on amplitude error following an overvoltage apply. Also, note that no power law calibration is applied to the protection class OVT output, thus giving a decreased accuracy, but over a greater dynamic range.

It has been possible to correct for the post-overvoltage behaviour of piezoelectric materials algorithmically in the interrogation software of previously developed sensors. The post-overvoltage increase in sensitivity of piezoelectric materials follows a predictable and repeatable decay curve and it should not prove to be a difficult task to perform the same algorithmic correction for the OVT.

Based on the results of the analysis presented here, it can be concluded that the OVT has the potential to offer combined metering and protection capability (using different calibrations, which can be output simultaneously) according to the requirements for protection classes specified by the IEC 60044-7 standard. Furthermore, the OVT meets the partial discharge requirements for VTs with  $U_m = 12$  kV. In future, a slightly more complex calibration procedure will make it possible for the OVT to meet the metering and protection accuracy limits with a single readout.

### 3.6 New calibration services for sensors with analogue output

The capabilities of existing NMI facilities for the calibration of conventional instrument transformers were extended to non-conventional sensors with analogue output signals, in order to address the demands for their traceable calibration. These signals are low currents in the range well below 1 A, or low voltage signals up to 10 V, whereas the signals from conventional instrument transformers are typically between 1 A and 5 A (for current transformers) or between 115 V and 120 V (for voltage transformers). Wideband sampling-based voltage ratio measurement system was adapted for these applications. The necessary infrastructure for traceable calibration of non-conventional sensors with analogue output was created, and respective CMC (Calibration and Measurement Capabilities) entries were submitted to EURAMET for inclusion into BIPM database. The target uncertainties, ratio error below 0.003 % and phase displacement below 0.003 crad were met.

Traceable calibration services were also developed for test sets used for calibration of the non-conventional sensors. Respectively, CMC entries were prepared with uncertainties of below 0.01 % for ratio error and 0.01 crad for phase displacement.

Three different methods for different users were developed for testing non-conventional sensors with analogue output. The work was performed jointly between METAS, VSL, TUBITAK and PTB.

**3.6.1 Modified conventional test-set**

The first approach relies on modifying the existing calibration system for conventional transformers to allow calibration of electronic voltage and current transformers (EVTs and ECTs) with analogue outputs at the power frequencies. Because the output voltages of analogue EVT and ECTs are too low for direct comparison with the secondary output of conventional transformers using traditional bridges, analogue outputs of such transducers must be amplified up to the traditional voltage or current levels. For this purpose, a voltage amplifier with an electronically compensated two-stage voltage transformer was developed for calibration of EVT (see Figure 29, left), and a transconductance amplifier based on an electronically compensated two-stage voltage-to-current converter was developed for calibration of ECTs (see Figure 29, right).

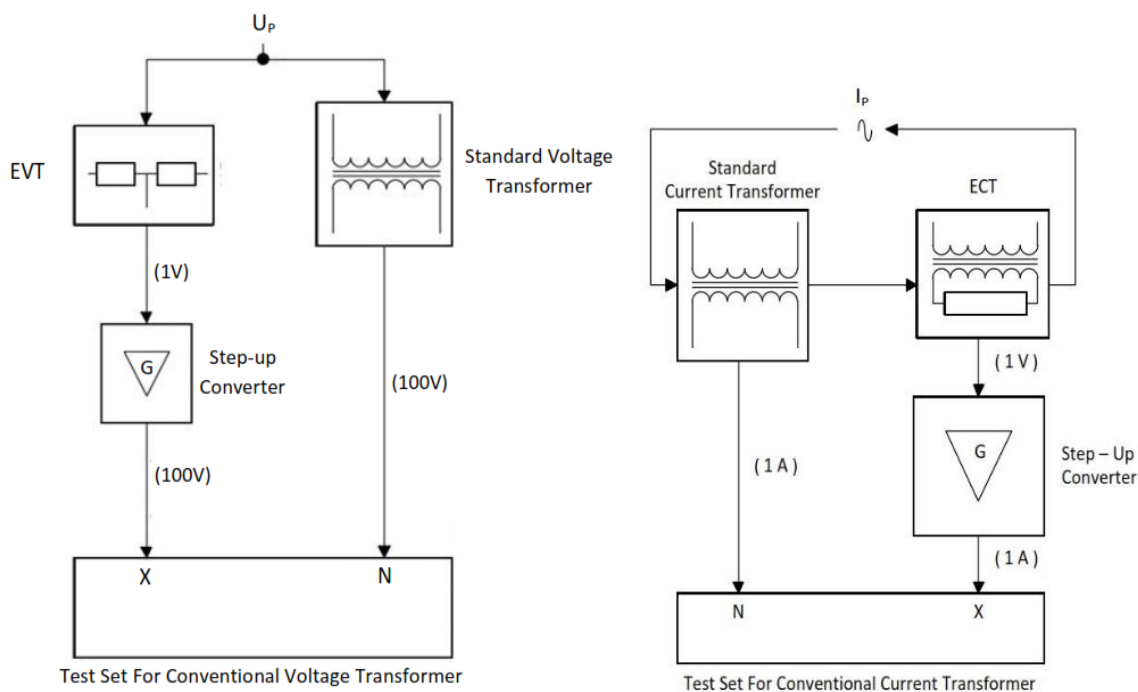


Figure 29 Setups for using conventional commercial test sets for calibration of EVT (left) and ECT (right).

**3.6.2 Sampler system**

The second developed method uses a sampling based system for testing non-conventional sensors with analogue output. The idea is to use precise high-resolution samplers to measure simultaneously the scaled secondary voltages both of the transformer under test and of the standard transformer. The measured voltages are used for calculating the rms voltages and the phase angles of the fundamental. From those results, the ratio error and the phase displacement of the transformer under test can be calculated. The setups for the sampler systems for calibration of EVT and ECTs is shown in Figure 30.

This approach is attractive for NMIs, where traceable characterization of each individual component can be made to obtain the highest precision.

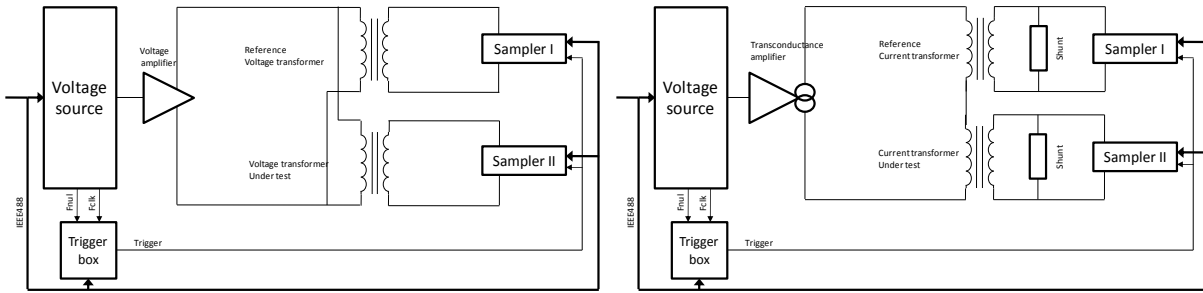


Figure 30 Setups for using sampling based method for calibration of EVT's (left) and ECT's (right).

The challenge lies in the precise scaling of the current and voltage to levels, which are suitable for the samplers.

The scaling of the voltage is done using a reference transformer and/or inductive voltage divider (IVD). To scale the voltage from the secondary 100 V to a more suitable voltage for the samplers, typical 1 V. The secondary of the non-conventional sensor needs to be scaled as well. This is done using an IVD.

### 3.6.3 Test-set for non-conventional sensors

The third method shown in Figure 31 uses a commercial test set for analogue non-conventional voltage and current sensors. It consists of a calibrated conventional voltage or current standard transformer, a sensor under test and a commercial test set for non-conventional sensors.

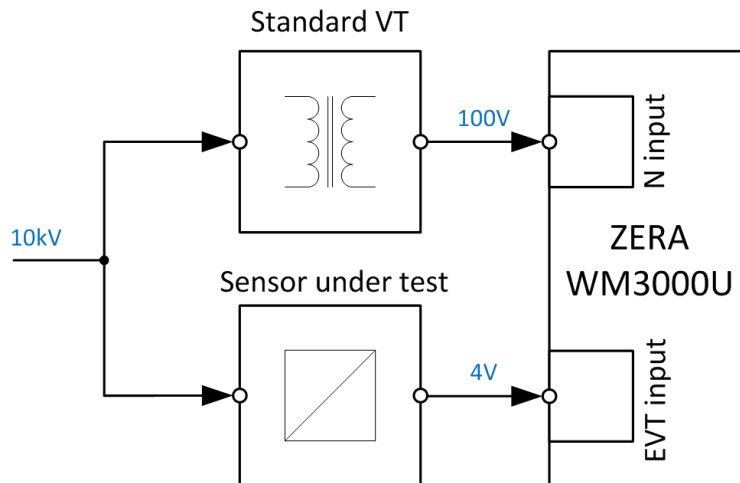


Figure 31 Setup for using a test sets for non-conventional analogue sensors for calibration of EVT's.

For testing the commercial test sets for non-conventional analogue sensors, ratio error and phase displacement values were applied to the device under test (DUT) and a reference bridge. By comparing the measurement results of the DUT and the reference bridge, the errors of the DUT can be calculated. The reference bridge, here, is a digital sampling wattmeter based ratio standard with 1 ppm resolution in both ratio error and phase displacement measurements.

Before this project, calibration and testing of non-conventional sensors with analogue output and the calibration of commercial test sets were not possible. Due to the work carried out within this project, the calibration/testing of the non-conventional sensors with analogue output is now possible with three different methods. The best uncertainties can be reached with the self-constructed sampled based method (10 ppm /  $\mu$ rad). This method is useful for NMIs. By using the old commercial test sets for conventional sensors with amplifiers and

commercial test sets for non-conventional analogue sensors, uncertainties below 100 ppm and 100 µrad can be reached. This method might be a practical and reliable calibration method for calibration/testing laboratories. The calibration of commercial test sets for non-conventional analogue current and voltage sensors has an uncertainty of < 10 ppm / µrad.

The result of this project are new CMC entries for calibrating non-conventional analogue current and voltage sensors and for calibrating test sets for non-conventional analogue current and voltage sensors for the first time.

### 3.7 New calibration services for sensors with digital output

New facilities for calibrating voltage and current sensors with digital output according to IEC61850-9-2 were established. To achieve this, the digital data must be compared to data obtained from a reference set-up using a traditional reference instrument transformer. This required the addition of a time stamp to the data from the reference set-up, and hardware and software to analyse the IEC61850-9-2 compliant data from the sensors. This time synchronisation was achieved with GPS modules or pulse per second (PPS) generators. Representative uncertainty budgets were developed for the SV protocol. The software platforms were designed and made available within the consortium to develop a common understanding of the issues involved.

Analogue conventional or non-conventional instrument transformers retrofitted with standalone merging units (SAMUs) were investigated using the software and hardware tools developed. SAMUs can be regarded as an analog-to-IEC61850-9-2 converter. Transformers can compare the known value with the value published by the SAMU. A test setup for non-conventional instrument transformers was developed, including generation of primary current and voltage signals of sufficient power to excite the sensors under test. A system capable of calibrating the sensors equipped with SV communication in substations was created.

Both the necessary infrastructure for traceable calibration of non-conventional sensors with digital output was created, and calibration services and associated CMC entries were created. The achieved uncertainties of 0.003 % for ratio error and 0.003 crad for phase displacement are low enough to meet industrial needs.

Infrastructure was also created for traceable calibration of test sets for digital output systems, and calibration services and CMC entries were prepared. The calibration uncertainties of 0.01 % for ratio error and 0.01 crad for phase displacement again satisfy industrial needs. The work on digital non-conventional sensor calibration was performed jointly between METAS, and PTB.

#### 3.7.1 Calibration of sensors with digital output

The developed calibration system for digital voltage and current sensors consists of a calibrated conventional voltage and current reference transformers, and a calibrated commercial test set for digital sensors. A system for calibration of digital voltage sensor is shown in Figure 32.

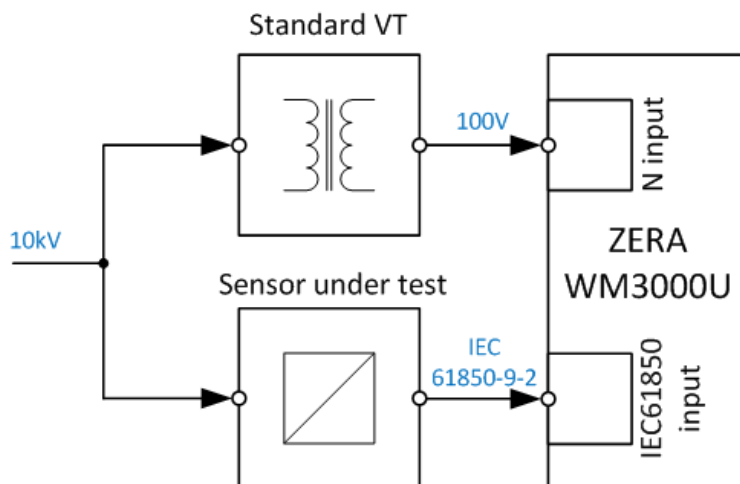


Figure 32 Calibration system for digital non-conventional voltage sensors

The system for calibrating one channel of a SAMU shown in Figure 33. In this system, a reference analogue signal is generated by an arbitrary waveform generator. This signal is amplified before being split in two different channels. One channel is the input for the SAMU, and the other is “reacquired” by a reference digitizer after it has been attenuated by a resistive divider (necessary not to exceed the digitizer’s input range). The reference digitizer is an NI PXI-4461 module mounted into a PXI chassis together with an NI PXI-6683 timing board. This serves as a reference signal. The SAMU simultaneously converts the amplified signal into SV with a fixed sampling frequency and sends them through the LAN. GPS receiver is used to tie the time of the Master Clock to UTC (Universal Coordinated Time).

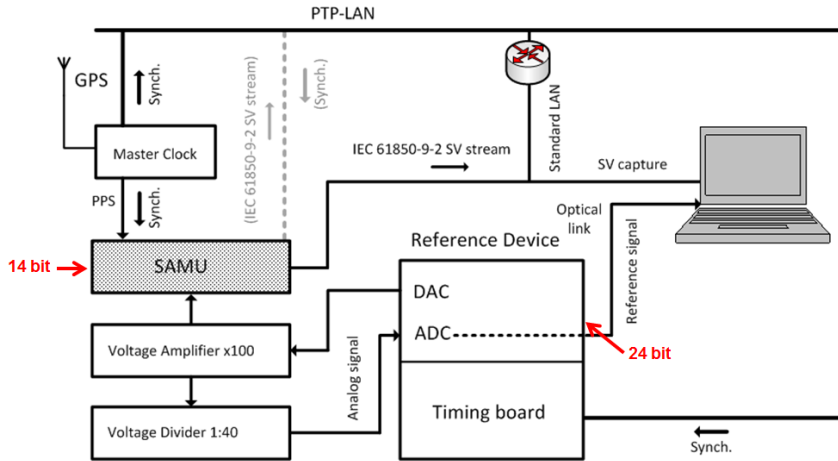


Figure 33 Structure of the measurement system for SAMU calibration.

### 3.7.2 Test-sets for calibration of sensors with digital output

For calibrating test sets for non-conventional sensors with digital output, two different methods were developed.

The first method is used for devices, where the analogue and digital signals are compared within the instrument. In this method, both precise analogue signals, and synthetic stream of sampled values according to IEC 61850-9-2, are created and compared with the device under test (DUT) according to Figure 34. The system is based on sampling power standard.

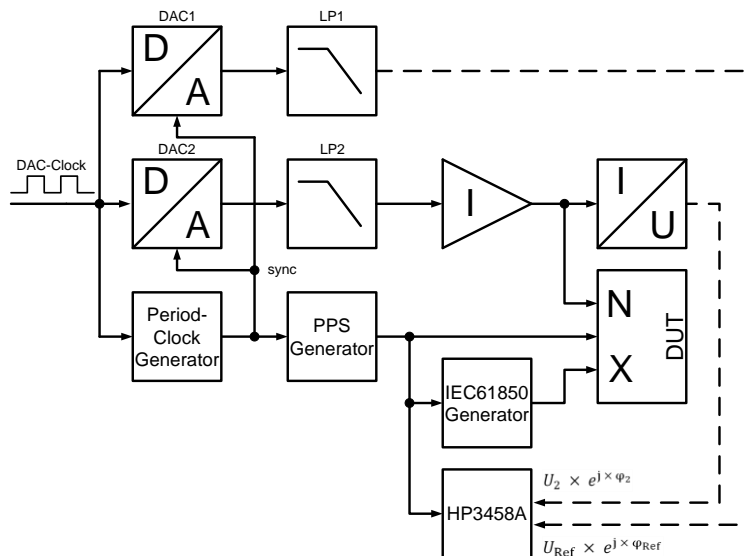


Figure 34 Setup for calibration of Zera type test sets. The bridge has inputs for both analogue and digital signals.

The synchronized digital-to-analogue converters (DAC1 and DAC2) generate two phase locked signals with  $\pm 10$  V amplitude and arbitrary phase angles. The output of each DAC is low pass filtered (LP) to remove quantization noise. DAC1 creates the phase reference signal to the sampling power reference (2 x HP3458A). The output signal from DAC2 is converted either to high voltage (for voltage sensor test set) or to high current (for current sensor test set). This emulates the signal from the secondary of a voltage or current transformer, and it is fed to the analogue input N of the DUT. Subsequently,  $I_N$  or  $U_N$  is precisely scaled to  $U_2$ , which is measured with a HP3458A sampling voltmeter. Knowing the characterized delay of DAC1, the absolute phase of the analogue signal fed to N input can be calculated.

The digital X signal, emulating the secondary output signal of a digital non-conventional instrument transformer, is generated with a sampled values generator. This device sends data of a pre-configured sinusoidal waveform over network using the IEC61850-9-2 protocol. Both DACs and the sampling power reference use a timing clock signal (DAC-clock) derived from stable frequency reference.

The second method is used for test sets, where the bridge generates the analogue signal (either voltage or current) together with respective reference data stream according to Figure 35. In this case the analogue signal from device under test (Test Set in Figure 35), is sampled by the ADC of the reference device, and the sampled reference signal is collected by a computer. The computer also captures the sampled value stream generated by the test set from local area network, and calculates the results for the calibration. An open source software platform is used for this purpose.

Both the test set under calibration, and the ADC are synchronized to PTP signal on the local area network.

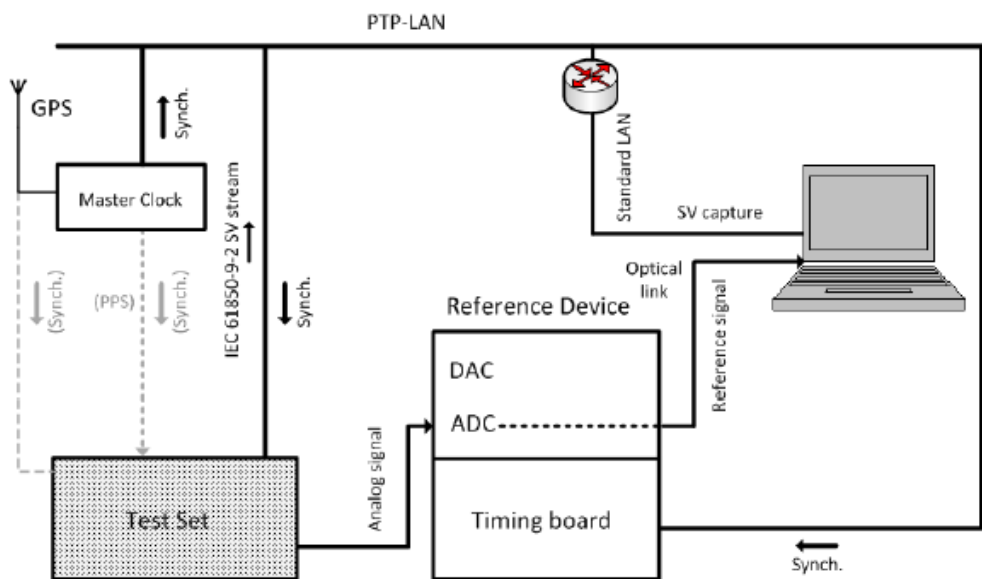


Figure 35 Setup for calibration of Omicron type test sets. The bridge generates both analogue and digital signals.

Before this project, calibration and testing of non-conventional sensors with digital output, SAMUs and the calibration of commercial test sets were not possible. Due to the work carried out within this project, the calibration/testing of the non-conventional sensors with digital output and SAMUs is now possible. The uncertainties for calibrating non-conventional digital current and voltage sensors and for test sets for non-conventional digital sensors are below 100 ppm for the ratio error and 100  $\mu$ rad for phase displacement.

The objectives of creating new CMC entries for calibration of non-conventional digital current and voltage sensors, and for respective test sets, were met.

### 3.8 Conclusion

#### *Design, manufacture and characterise a wideband sensor based on the optical Faraday effect*

A fibre optic current sensor (FOCS) is a current sensor used for measuring direct current (DC), and is based on the Faraday effect, which describes the interaction between optical and magnetic properties. The project investigated possible solutions for the FOCS design, and a mathematical model was developed to describe the behaviour of the Faraday effect in a fibre. Two improvements to the designs were introduced: working on shorter wavelengths, and doping of the sensing fibre. To eliminate effects from effects from vibration, acoustic coupling and temperature changes, an all-fibre FOCS system was designed and built. Unfortunately, obtaining suitable fibres to reach the targets was more difficult than anticipated so only shorter wavelength (650 nm) operation was demonstrated.

The objective was to perform on-site calibrations with an uncertainty below 100  $\mu\text{A/A}$  (0.01 %). However, the uncertainty demonstrated by the end of the project is 1 % in the range from 400 A to 3500 A, in laboratory conditions. The full capability of the new design could not be fully explored during the project.

#### *Magnetic shielding technique on Rogowski coil*

Rogowski coils are well recognised as current sensors and are suited for high-voltage applications. However, one of their weak points is the unwanted coupling of external currents near the coil and sensitivity to position. Hence, we aimed to reduce the immunity of a Rogowski coil against these effects by more than factor of 10.

The metrological performance of the Rogowski coil developed by the project was characterised and immunity to the effects was reduced by factor of 100. The performance of the coil was demonstrated in calibration setups on medium and high voltage levels. Together with temperature compensation techniques, the measurement uncertainties were reduced to less than 100  $\mu\text{A/A}$  for ratio and 100  $\mu\text{rad}$  for phase displacement. The temperature dependence of the ratio was less than 5  $\mu\text{A/A/K}$ . The drawbacks of the new design for the Rogowski coil are increased weight and reduced dynamic range.

The Rogowski coil has the potential to be a good tool for NIMs and calibration laboratories for measuring current and its harmonics, although it is not yet at the point of commercialisation.

#### *Improved precision voltage sensor*

A precision voltage sensor was developed for the measurement of voltage and power quality. The sensor was designed for direct connection to medium voltage switchgear. The uncertainty of the scale factor is less than 100  $\mu\text{V/V}$  (0.01 %) up to 1 kHz, and 0.2 % up to 10 kHz. The improved precision voltage compact sensor enhances power quality measurements, without compromising the accuracy of the measurement of the fundamental components.

The objectives of an uncertainty below 100  $\mu\text{V/V}$  and bandwidth of 5 kHz were met and the improved precision voltage sensor is close to commercialisation.

#### *Traceability for new non-conventional techniques not yet commercially available*

A current clamp for monitoring power quality on medium and high voltage lines was developed. The clamp can be used for the measurement of currents on the ground terminal of existing capacitors on the power network. The measurement range of the compensated current clamp is from 15 mA to 9.6 A, and the uncertainty, including the digitiser system, was found to be less than 0.1 % in laboratory environment. The bandwidth of the current clamp is 100 kHz.

The objective of demonstrating measurement of voltage harmonics with uncertainty below 0.2 % using a current clamp was met by the project. The technology for using current clamp for traceable measurements of harmonic voltages in medium and high voltage networks is now ready for wider application.

Optical voltage and current (1 kA) transducers for distributed voltage measurements on medium-voltage networks (11 kV) based on fibre Bragg techniques were designed and constructed. The current transducers and interrogation system met the accuracy requirements for protection devices, as predicted by pre-manufacture simulation. The optical voltage transducers met the target accuracy (0.2 % in ratio error and 0.3 crad in phase displacement) in laboratory conditions, when they were not subjected to transient overvoltages.

The interrogation system has the potential for differential fault detection in power lines, due to its inherently simultaneous readout of multiple sensors. However, the fibre Bragg interrogation technique still needs further development before it can be applied for on-line measurement.

#### *Frequency responses of conventional and non-conventional sensors*

The differences in frequency responses of conventional and non-conventional sensors were studied. The measurement results confirmed that the tested non-conventional sensors had in general much better frequency response than conventional voltage instrument transformers. In contrast, the frequency responses of non-conventional current sensors and conventional current instrument transformers did not significantly differ.

#### *Applicability for measurements on existing substations*

The project was able to test some, but not all of the newly designed sensors on existing substations. The Rogowski coil design was used for medium and high voltage calibration demonstrations in laboratory conditions, but not in-service.

The current clamp was tested on-site and in-service in medium voltage network. The precision voltage sensor passed the tests required by insulation coordination standards for connection to medium voltage network, and its performance was demonstrated on-site and in-service in medium voltage network. Development of fibre Bragg grating based sensors progressed up to insulation testing, but their demonstration in on-site conditions was not possible during the project. The development of the optical current sensor proceeded only to laboratory demonstration stage, rather than the planned on-site measurements.

#### *New services for calibration of non-conventional sensors with analogue or digital output*

Calibration setups were prepared for test systems for analogue and digital non-conventional sensors. The developed calibration setups are based either on sampling measurement system, or on a commercial test set. A test system was developed for commercially available test sets for conventional and non-conventional transformers. The systems have been used for calibrations at partners PTB, VSL and TUBITAK, and respective updates on their official calibration scope have been either completed or initiated.

Two Good Practice Guides were developed, one providing guidance for realisation of calibration setups for non-conventional sensors and test sets by METAS, VSL, TUBITAK, PTB and TU Dresden, and the other discussing accuracy of installation of non-conventional sensors by TU Dresden and PTB.

The objective to develop new calibration services for non-conventional sensors and their test-systems was achieved and it is now possible to provide traceability for calibration of sensors that have an analogue input and a digital output. This is particularly important as substations become increasingly digital and the instrument manufacturers require calibration for the digital equipment.

## 4 Actual and potential impact

### 4.1 Dissemination

The project results were disseminated widely to the stakeholder community via 21 publications, 9 posters, 5 presentations and the project website at <http://futuregrid.emrp.eu/>. Two workshops were held to attract stakeholders from industry. The workshop in 2016 was arranged jointly with the EMPIR project 14IND08 [Metrology for the electrical power industry](#) and attracted 40 people representing project partners, standardisation organisations, industry and academia. During this one-day workshop, 23 posters and 12 oral presentations were presented including a keynote speech. The final dissemination workshop in 2017 was organised with two other EMRP projects ENG52 [Measurement tools for Smart Grid stability and quality](#) and ENG63 [Sensor network metrology for the determination of electrical grid characteristics](#). About 70 people from 17 different countries attended the two-day event. The FutureGrid session of the workshop featured 10 presentations and a panel discussion. The workshops provided new insights for the participants regarding measurement capabilities of non-conventional instruments. The presentations of the workshops are available on the project website <http://futuregrid.emrp.eu/>

Two Good Practice Guides for application and calibration of non-conventional sensors were developed by the project: '(1) Recommendations related to the calibration and testing of non-conventional current and voltage sensors to support European and national standardisation groups' and '(2) The installation of non-conventional sensors in order to ensure high accuracy', which are available for download on the project website until the end of 2018.

### 4.2 Metrological achievements

This project has significantly contributed to the promotion, development, improvement and assessment of novel sensor technologies in future power networks. The project has provided novel field-deployable instruments for current and voltage control and on-site calibration as well as for power quality measurements on high voltage grids. The developed tools allow traceable measurements to control power grids. This is coming increasingly important as growing number of distributed sources are connected to power networks causing power quality degradation.

The main impact from the project is the provision of new services, which have been established for calibration of digital and analogue non-conventional voltage and current transformers. The calibration services will provide a means for manufacturers to prove the performance of their new products. New CMC entries for calibration of analogue non-conventional transformers were submitted to EURAMET by PTB, VSL and TUBITAK, and for calibration of digital output transformers by PTB and METAS.

### 4.3 Early impact

#### 4.3.1 User uptake

The following new calibration services were established as a result of the project:

- Calibration services for non-conventional current and voltage sensors by PTB, VSL, TUBITAK and METAS
- Calibration services for digital output current and voltage sensors and respective test sets by PTB, VSL, TUBITAK and METAS

Wider application of the developed new technologies is supported by the following actions:

- The project triggered development of new type of sensing fibre for optical current transformers at the University of Southampton.
- FFII, a project partner, is working towards commercialisation of the medium voltage probe.
- The medium voltage probe is proposed as reference measurement device for the EMPIR project 16ENG04 MyRailS

- TUBITAK used the developed Rogowski coil for calibration of customer's medium voltage current transformer.
- PTB has performed calibration of non-conventional sensors for customers.
- PTB has discussed findings of a commercial device with the manufacturer in order to fix issues in the device software.
- SMU supported development of a commercial version of openable Rogowski coil for measurements on medium voltage network
- CMI supported development of shielding for Rogowski coil by placing ferromagnetic materials near the coil.

### 4.3.2 Standards

The project contributed to the ongoing work of a number of standardisation committees and work groups, both at the international and national levels. Internationally this included contributions to the CEN/CENELEC STAIR (STAndardisation, Innovation and Research) strategic working group, IEC TC 38 (instrument transformers) and TC 42 (high voltage and current testing and measurement techniques), and their working groups. At the national level, contributions were made to IEC TC 115 (High Voltage Direct Current (HVDC) transmission for DC voltages (above 100 kV), TC 13 (Electrical energy measurement), and AENOR CTN207 (Electric Power Transmission and Distribution). Project partners also contributed to IEC working groups dealing with instrumentation for high-voltage and high-current testing, and with uncertainty in instrument transformer calibration.

Pre-standardisation work included active participation to CIGRE (Conseil International des Grands Réseaux Electriques), Council on Large Electric Systems) general sessions and technical working groups on atmospheric influence on spark over voltage, and on measurement techniques for fast transients.

Metrology policies were influenced by attendance to EURAMET TC-EM (Technical Committee on Electricity and Magnetism) meetings. In addition, project members were active on the BIPM Consultative Committee for Electricity and Magnetism (CCEM) ad hoc working group on revising high voltage related service categories.

### 4.4 Potential impact

Introduction of non-conventional sensors developed in the project will facilitate the integration of alternative sustainable energy sources necessary to meet the EU's 2020 target of a 20 % of reduction in greenhouse gas emissions. Introduction of the new technologies will reduce grid operators' problems in management of the network, and improve grid stability even when many new types of energy sources are introduced.

Reducing power transmission losses can only be achieved by higher precision and lower uncertainty measurements of power quality and energy loss. Equipment and procedures for calibration of the new non-conventional sensors developed in the project support this progress. It is estimated that average losses in the electricity grid are in the order of 10 % from generation to consumption points. Total electricity production in the European Union was for 2012 about 3000 TWh. If the efficiency of 5 % of the generation is improved by 2 %, the net gain would be 0.1 % of 500 000 M€, which is 500 M€.

### 5 Website address and contact details

#### 5.1 Project website address: <http://futuregrid.emrp.eu/>

Information on the project (project description, events, publications, newsletters, reports, etc.) for project partners and stakeholders.

#### 5.2 Contact details

For further information on the project, contact Jari Hällström, VTT, [jari.hallstrom@vtt.fi](mailto:jari.hallstrom@vtt.fi).

For further information on wideband sensor based on optical Faraday effect, Alf-Peter Elg, RISE, [alf.elg@ri.se](mailto:alf.elg@ri.se).

For further information on magnetic shielding technique on Rogowski coil, Burak Ayhan, TUBITAK, [burak.ayhan@tubitak.gov.tr](mailto:burak.ayhan@tubitak.gov.tr).

For further information on precision voltage sensor, Jorge Rovira, FFII, [JRovira@lcoe.etsii.upm.es](mailto:JRovira@lcoe.etsii.upm.es).

For further information on traceability for non-conventional techniques, contact Enrico Mohns, PTB, [enrico.mohns@ptb.de](mailto:enrico.mohns@ptb.de).

For further information on new calibration services for non-conventional sensors, contact Enrico Mohns, PTB, [enrico.mohns@ptb.de](mailto:enrico.mohns@ptb.de); Burak Ayhan, TUBITAK, [burak.ayhan@tubitak.gov.tr](mailto:burak.ayhan@tubitak.gov.tr); Marco Agustoni, METAS, [marco.agustoni@metas.ch](mailto:marco.agustoni@metas.ch); or Ernest Houtzager, VSL, [ehoutzager@vsl.nl](mailto:ehoutzager@vsl.nl).

## 6 List of publications

1. G. Fusiek, P. Orr, and P. Niewczas, "Reliability of an all-optical differential current detection technique during environmental temperature perturbations", Proceedings of IEEE SENSORS 2014, Page(s): 1121–1124, DOI: 10.1109/ICSENS.2014.6985203.
2. G. Fusiek, P. Orr, and P. Niewczas, "Temperature-Independent High-Speed Distributed Voltage Measurement using Intensiometric FBG Interrogation", Proceedings of IEEE I2MTC 2015, Page(s): 1430–1433, DOI: 10.1109/I2MTC.2015.7151486.
3. J. Hlavacek, K. Draxler and R. Styblikova: "20 kV AC Divider with Ratio Correction", The 19th International Symposium on High Voltage Engineering, Pilsen, Czech Republic, August, 23– 8, 2015.
4. E. Mohns, S. Fricke, C. Jäschke and P. Schegner: "A Current Clamp based High Voltage Monitoring System", 6rd IEEE International Workshop on Applied Measurements for Power Systems, AMPS 2015, September 2015, Aachen, Germany.
5. G. Fusiek and P. Niewczas, "Laboratory investigation of an intensiometric dual FBG-based hybrid voltage sensor", Proc. SPIE 9634, 24th International Conference on Optical Fibre Sensors, 96341H, September 28, 2015; doi:10.1117/12.2195025.
6. D. Istrate, R. Etienne, J. Dubard, A. Litwin, O. Enouf: "Determination of the Verdet Constant of Low Birefringence Single-Mode Optical Fiber", CPEM 2016 Digest, Ottawa, July 2016; DOI: 10.1109/CPEM.2016.7540523.
7. E. Houtzager; E. Mohns; S. Fricke; B. Ayhan; T. Kefeli; H. Çaycı: "Calibration systems for analogue non-conventional voltage and current transducers", CPEM 2016 Digest, Ottawa, July 2016; DOI: 10.1109/CPEM.2016.7540488.
8. M. Agustoni, A. Mortara: "A Calibration Setup for IEC 61850-9-2 Test Sets", CPEM 2016 Digest, Ottawa, July 2016; DOI: 10.1109/CPEM.2016.7540644.
9. E. Mohns, S. Fricke, and F. Pauling: "An AC Power Amplifier for Testing Instrument Transformer Test Equipment", CPEM 2016 Digest, Ottawa, July 2016; DOI: 10.1109/CPEM.2016.7540559.
10. J. Nelson, G. Fusiek, L. Clayburn, P. Niewczas, C. Booth, P. Orr, N. Gordon: "Development and testing of optically-interrogated current sensors," Proceedings of AMPS 2016, Aachen, Germany, September 2016; DOI: 10.1109/AMPS.2016.7602871.
11. D. Tzelepis, A. Dysko, G. Fusiek, J. Nelson, P. Niewczas, D. Vozikis, P. Orr, N. Gordon, and C. Booth, "Single-End Differential Protection in MTDC Networks Using Optical Sensors", IEEE Trans. Power Del. (accepted), DOI 10.1109/TPWRD.2016.2645231.
12. M. Agustoni and A. Mortara, "A Calibration Setup for IEC 61850-9-2 Test Devices," IEEE Trans. Instrum. Meas., vol.66, no.6, pp.1124-1130; DOI: 10.1109/TIM.2017.2665938.
13. H.G. Latzel und E. Mohns: "Kapitel 18 - Prüftechnik für Messwandler", in M. Kahmann, P. Zayer, M. Arzberger (Eds.): "Handbuch Elektrizitätsmesstechnik", 3. Auflage 2017, ISBN 978-3-8007-4403-9, E-Book: ISBN 978-3-8007-4405-3
14. Draxler,K.; Styblikova, R.: Magnetic Shielding of Rogowski Coils, Proc. of I2MTC 2017 Conference, Torino 2017, p.p. 1467 – 1471.
15. Draxler,K.; Styblikova, R.: Calibration of AC clamp Meters, IEEE Transactions on Instrumentation and Measurement, 2016, 65(5), 1156-1162. ISSN 0018-9456.
16. K. Draxler, R. Prochazka, J. Hlavaček, M. Knenicky and R. Styblikova, "Use of a nanocrystalline core for a precise non-invasive AC current measurement," 2016 Conference on Precision Electromagnetic Measurements (CPEM 2016), Ottawa, ON, 2016, doi: 10.1109/CPEM.2016.7540492
17. F. Garnacho, A. Khamlichi, J. Rovira, "The Design and Characterization of a Prototype Wideband Voltage Sensor Based on a Resistive Divider," Sensors 2017, 17, 2657, doi: 10.3390/s17112657.